Lymphocyte-derived exosomal microRNAs promote pancreatic beta cell death and may contribute to type 1 diabetes development

Claudiane Guay, Janine K. Kruit, Sophie Rome, Veronique Menoud, Niels L. Mulder, Angelika Jurdzinski, Francesca Mancarella, Guido Sebastiani, Alena Donda, Bryan J. Gonzalez, et al.

Graphical Abstract

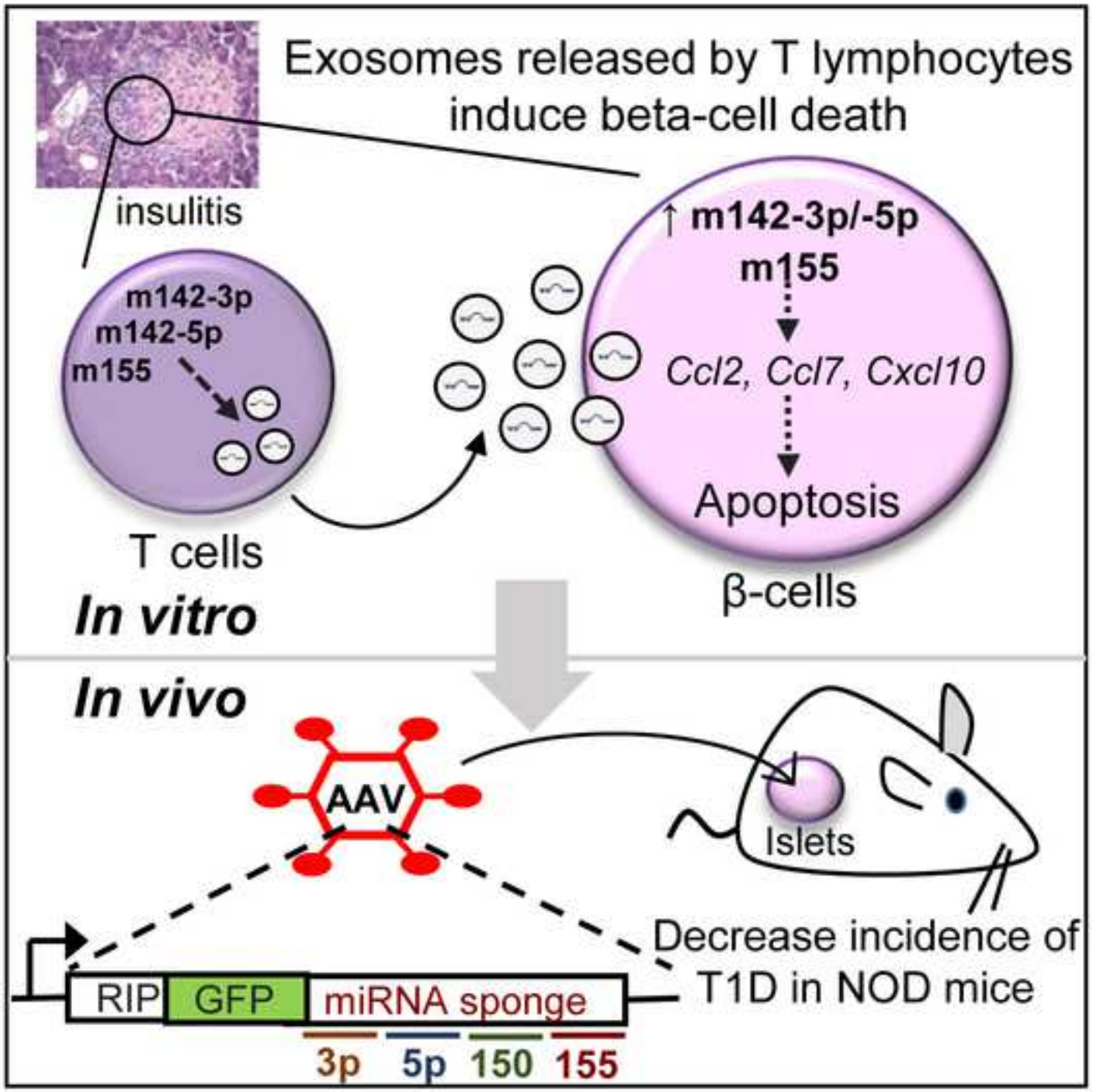

Lymphocyte-derived exosomal microRNAs promote pancreatic β-cell death and may contribute to type 1 diabetes development

Running title: Role of exosomal microRNAs in type 1 diabetes

Claudiane Guay[1], Janine K. Kruit[2], Sophie Rome[3], Véronique Menoud[1], Niels L. Mulder[2], Angelika Jurdzinski[2], Francesca Mancarella[4,5], Guido Sebastiani[4,5], Alena Donda[6], Bryan J. Gonzalez[1,7], Camilla Jandus[8], Karim Bouzakri[9], Michel Pinget[9], Christian Boitard[10-11], Pedro Romero[6], Francesco Dotta[4,5], and Romano Regazzi*[1]

[1] Department of Fundamental Neurosciences, University of Lausanne, Lausanne, Switzerland

[2] Department of Pediatrics, Section Molecular Metabolism and Nutrition, University of Groningen, University Medical Center Groningen, Groningen, the Netherlands

[3] CarMeN laboratory (INSERM 1060, INRA 1362, INSA), University of Lyon, Faculté de Médecine de Lyon Sud, France

[4] Diabetes Unit, Department of Medicine, Surgery and Neurosciences, University of Siena, Siena, Italy

[5] Umberto Di Mario ONLUS Foundation - Toscana Life Science Park, Siena, Italy

[6] Ludwig Center for Cancer Research, University of Lausanne, Lausanne, Switzerland

[7] current address: Naomi Berrie Diabetes Center & Department of Pediatrics and Medicine, College of Physicians and Surgeons, Columbia University, New York, USA

[8]Department of Oncology, CHUV, University of Lausanne, Lausanne, Switzerland

[9] UMR DIATHEC, EA 7294, Centre Européen d'Etude du Diabète, Université de Strasbourg, Fédération de Médecine Translationnelle de Strasbourg, Strasbourg, France

[10] Institut National de Santé et de Recherche Médicale U1016, Paris, France

[11] Université Paris Descartes, Sorbonne Paris Cité, Paris, France

*Corresponding author and Lead contact: Dr. Romano Regazzi

Department of Fundamental Neurosciences

Rue du Bugnon 9, 1005 Lausanne, Switzerland

Tel. ++41 21 692 52 80/Fax. ++41 21 692 52 55

E-mail: Romano.Regazzi@unil.ch

SUMMARY

Type 1 diabetes is an autoimmune disease initiated by the invasion of pancreatic islets by immune cells that selectively kill the β-cells. We found that rodent and human T lymphocytes release exosomes containing the microRNAs miR-142-3p, miR-142-5p and miR-155 which can be transferred in active form to β-cells favoring apoptosis. Inactivation of these miRNAs in recipient β-cells prevents exosome-mediated apoptosis and protects NOD mice from diabetes development. Islets from protected NOD mice display higher insulin levels, lower insulitis scores and reduced inflammation. Looking at the mechanisms underlying exosome action, we found that T lymphocyte exosomes trigger apoptosis and the expression of genes involved in chemokine signaling, including *Ccl2*, *Ccl7* and *Cxcl10*, exclusively in β-cells. The induction of these genes may promote the recruitment of immune cells and exacerbate β-cell death during the autoimmune attack. Our data point to the exosomal-miRNA transfer as a communication mode between immune and insulin-secreting cells.

Keywords: Exosomes, microRNAs, pancreatic β-cells, T lymphocytes, type 1 diabetes, cell-cell communication.

INTRODUCTION

Type 1 diabetes (T1D) is an autoimmune disorder characterized by infiltration of the islets of Langerhans by immune cells and by selective elimination of the insulin-secreting β-cells (Eizirik et al., 2009). The infiltration of immune cells has been observed in non-obese diabetic (NOD) mice, a well-known model of T1D (Anderson and Bluestone, 2005; Atkinson and Leiter, 1999), but also in the islets of human diabetic donors (Atkinson et al., 2014; Krogvold et al., 2016; Lundberg et al., 2017). Patients suffering from T1D require lifelong insulin administration to regulate whole body glucose metabolism and homeostasis. Understanding the dialogue between pancreatic β-cells and the infiltrating immune cells is crucial to promote the design of novel strategies to prevent the development of this disease and/or to find a cure.

Part of the detrimental effects of the immune cells on β-cell survival is known to be exerted through the release of pro-inflammatory cytokines (Eizirik et al., 2009). However, lymphocytes were recently found to release another class of immune mediators: the exosomes (Thery et al., 2009). Exosomes are small extracellular vesicles of 50-150 nm of diameter that originate from the late endosomal pathway and are secreted in the extracellular space upon fusion of multivesicular bodies with the plasma membrane (Thery et al., 2009). Exosomes are released by numerous cell types, including lymphocytes and pancreatic islets (Guay and Regazzi, 2015; Robbins et al., 2016), and are present in the blood and other body fluids (Weber et al., 2010). These extracellular vesicles transport proteins, mRNAs and non-coding RNAs that can be transferred in active form to recipient cells, suggesting an important role in cell-to-cell communication (Kosaka et al., 2010; Thomou et al., 2017; Valadi et al., 2007; Zhang et al., 2010). Until recently, most of the studies on exosomes were performed *in vitro* or in *ex vivo* cell models, but *in vivo* studies are now emerging. For example, the use in mice of the Cre-loxP system or of a human-specific miRNA elegantly demonstrated the transfer of the exosome cargo between distally located cells (Ridder et al., 2014; Thomou et al., 2017; Zomer et al.,

2015). Of interest, the transfer of nucleic acids by exosomes was found to be promoted by inflammatory conditions (Ridder et al., 2014).

MicroRNAs (miRNAs) constitute one of the main cargoes transported by exosomes. These small non-coding RNAs are key post-transcriptional modulators of gene expression and can be transferred in active form via exosomes to acceptor cells (Kosaka et al., 2010; Montecalvo et al., 2012; Thomou et al., 2017; Valadi et al., 2007; Zhang et al., 2015). MiRNAs play an important role in the control of β-cell activities. Indeed, they are involved in the differentiation and functional maturation of β-cells and regulate insulin secretion and cell survival (Dumortier et al., 2013; Eliasson and Esguerra, 2014; Guay et al., 2011; Jacovetti et al., 2015; Lynn et al., 2007). Deregulation of miRNA expression has been associated with the development of T1D and T2D and with age-associated decline in β-cell proliferation (Filios and Shalev, 2015; Guay and Regazzi, 2016; Nesca et al., 2013; Tugay et al., 2016). Moreover, some miRNAs were found to induce β-cell dysfunction and death under inflammatory conditions in both rodent and human islets (Grieco et al., 2017; Roggli et al., 2012).

In the present study, we investigated the involvement of miRNAs in the initial phases of T1D development in NOD mice. We found that islet insulitis is associated with an exosome-mediated transfer of a particular group of miRNAs, namely miR-142-3p, miR-142-5p and miR-155, from lymphocytes to β-cells, resulting in the selective death of the insulin-secreting cells. *In vitro*, inactivation of these miRNAs inside the β-cells protected them against apoptosis induced by T lymphocyte exosomes and, *in vivo*, prevented T1D development in NOD mice. Taken together, our results suggest that the transfer of miRNAs mediated by exosomes released by lymphocytes contributes to the destruction of the β-cells and could be part of the mechanisms leading to T1D development.

RESULTS

Increased abundance of miR-142-3p, miR-142-5p and miR-155 in β-cells of pre-diabetic NOD mice.

In a previous study, we performed a global miRNA expression profiling of pancreatic islets of 4 and 8 weeks-old female NOD mice (which correspond to control and pre-diabetic state, respectively) to understand the role of miRNAs in β-cell death associated with T1D development (Roggli et al., 2012). At 8 weeks of age, NOD mice are still normoglycemic but T lymphocytes are starting to infiltrate the islets (Roggli et al., 2012). The miRNAs displaying the most important deregulation in the islets of 8 weeks old animals were miR-142-3p/-5p, miR-150 and miR-155, which are known to control the activity of immune cells (Dudda et al., 2013; Kroesen et al., 2015; Wu et al., 2007) but are normally expressed at very low levels in insulin-secreting cells. Indeed, we found that these miRNAs are much more abundant in lymphocytes compared to islet cells (Figure S1A). The expression of these miRNAs is modified to a much lesser extent in the islets of age-matched diabetes-free NOD-SCID mice (Figure 1A), indicating that the changes observed in pre-diabetic mice are most likely linked to the development of the disease. The increase in the levels of miR-142-3p/-5p and miR-155 were detected also in FACS-sorted β-cells of pre-diabetic NOD mice (Figure 1B), confirming that the rise of these miRNAs occurs in insulin-secreting cells. In agreement with previous findings in rat islets (Bravo-Egana et al., 2012), the expression of these miRNAs was not affected by incubation of control C57Bl/6N mouse islets with the pro-inflammatory cytokines IFNγ, TNFα and IL-1β (Figure 1C). Therefore, the increase of miR-142-3p/-5p and miR-155 in β-cells in 8 weeks old NOD mice is unlikely to be caused by cytokines secreted by immune cells infiltrating the islets.

T lymphocytes release exosomes containing miR-142-3p, miR-142-5p and miR-155.

Since immune cells release large amounts of exosomes, we hypothesized that the rise of miR-142-3p/-5p, and miR-155 in islet cells of pre-diabetic animals may result from an exosome-mediated transfer favored by the proximity of T lymphocytes and β-cells during the initial phases of the disease. To

explore this hypothesis, we isolated by ultracentrifugation the vesicles released by human Jurkat T cells (exoT) and by $CD4^+/CD25^-$ T lymphocytes of NOD mice (exoNOD). Analysis of these preparations by electron microscopy (Figure 2A-B) and Nanosight technology (Figure 2D-E) revealed the presence of round-shaped small extracellular vesicles surrounded by a lipid bilayer membrane with a diameter of 50-200 nm. These small extracellular vesicles carried the characteristic exosomal markers CD81, Alix and Tsg101 (Thery et al., 2009) (Figure 2C). We next investigated if these small extracellular vesicles can be efficiently internalized by insulin-secreting cells. After an overnight incubation, DiD-labelled exoT were found to be taken up by most cells of the β-cell line MIN6B1 (Figure 2F).

We next examined the miRNA content of T cell exosomes. All three miRNAs, miR-142-3p/-5p and miR-155, were found to be present in the extracellular vesicles released by T lymphocytes (Figure S1B-C). To ensure that these miRNAs are confined inside exosomes, the samples were treated with RNase. In contrast to a synthetic oligonucleotide (miR-29a mimic) spiked into the samples, the level of the endogenous miRNAs was not affected by the RNase treatment and were degraded only when the exosome membrane integrity was altered with the detergent Triton X-100 (Figure 2G).

Exosomal miRNAs from T lymphocytes are transferred to β-cells.

To assess whether the miRNAs present in the exosomes of T lymphocytes can be transferred to β-cells, dispersed mouse islet cells were incubated with exoNOD for 72h (Figure 3A). This treatment led to a significant increase in the abundance of miR-142-3p/-5p and miR-155 in islet cells (Figure 3B). Similar results were obtained when MIN6B1 or rodent islet cells were exposed to exoT (Figure 3C and Figure S2B). The sequence of miR-142-3p and miR-142-5p is identical in humans and rodents and, therefore, it is not possible to distinguish the miRNAs delivered via the exosomes from those endogenously produced in mouse or rat β-cells. In contrast, human miR-155 (hsa-miR-155) differs by one nucleotide from its rodent counterparts (Figure S2A) and can be readily distinguished by qPCR

using species-specific primers (Table S1). This strategy enabled us to show that the rise of miR-155 observed in the receiving rodent islet cells is entirely due to an exosome-mediated transfer of hsa-miR-155 from the human Jurkat T cell line and not from an increase synthesis of endogenous mmu-miR-155 (Figure 3C-D and Figure S2C). This finding was further confirmed using exosomes purified from $CD4^+/CD25^-$ T cells of miR-155 knock-out mice (Figure S2D-E). Indeed, while the other miRNAs were still increased in recipient MIN6B1 cells, the level of miR-155 remained unchanged upon incubation with exosomes isolated from miR-155 knock-out mice (Figure S2F-H). To demonstrate that hsa-miR-155 is transferred in active form inside the β-cells, the receiving cells were transfected with a luciferase sensor. As expected the incubation of MIN6B1 cells with exoT for 48h or 72h led to a decrease in the luciferase activity of the hsa-miR-155 sensor (Figure 3E), confirming that the miRNA is transferred in active form in the receiving cells. Taken together, these results provide evidence for an exosome-mediated transfer of miRNAs from immune cells to β-cells analogous to that observed in other biological processes (Ridder et al., 2014; Thomou et al., 2017; Zhang et al., 2015).

T lymphocyte exosomes promote β-cell apoptosis and induce the upregulation of genes involved in cytokine and chemokine signaling.

We next investigated the impact of T lymphocyte exosomes on β-cell function and survival. Incubation of β-cells in the presence of exoT did not affect insulin secretion or content (Figure S3A-D) but led to a significant increase in cell apoptosis, which was prevented by the pan-caspase inhibitor zVAD (Figure 3F-G and Figure S3E-F). The cytotoxic action of T cell exosomes was reproduced in dispersed mouse islet cells incubated with exosomes from T cells of NOD mice (Figure 3H). The apoptotic effect of exoT cannot be attributed to the presence of residual traces of cytokines released by lymphocytes. In fact, incubation of β-cells in the medium surrounding the purified exosomes did not modify the level of the miRNAs and did not affect the survival of the cells (Figure S3G-H). To determine if this process occurs also in human, human islet cells were incubated with exosomes (exo-hT) of $CD4^+$ T cells

isolated from human blood donors. Similar to the findings obtained in rodents, exposure of human islet cells to exo-hT resulted in the transfer of miR-142-3p, miR-142-5p and miR-155 (Figure 3I) and in an increase in cell death measured by Hoechst or by TUNEL staining (Figure 3J-K).

Interestingly, the cytotoxic effect of the exosomes was restricted to β-cells. Indeed, the increase in apoptosis was reproduced in FACS-sorted rat β-cells (98±2% purity) but not in an α-cell-enriched fraction (91±4% α-cells) (Figure 4A-B). To assess whether this cell-specific effect is due to a selective uptake of the exosomes, we took advantage of the auto-fluorescence properties of the rodent β-cells (Kohler et al., 2012). Image Stream Flow Cytometry, revealed that DiD-labelled exoT can be equally detected in auto-fluorescent β-cells and in non-fluorescent islet-cells (Figure 4C). Consistent with these findings, upon incubation with exoNOD miR-142-3p, miR-142-5p and miR-155 were transferred to both FACS-sorted α- and β-cells (Figure 4D-E, respectively).

To elucidate the mechanisms through which T-cell exosomes exert their effect on β-cells, we analyzed by microarray the changes in the mRNA profile elicited in mouse islet cells by exoNOD. Upon exposure to exoNOD, we detected about 90 up-regulated and 20 down-regulated genes (nominal p-value < 0.05 and fold change > 2) (Table S2). Pathway analysis revealed a significant enrichment for genes involved in cytokine and chemokine signaling, including *Ccl2*, *Ccl7* and *IFNg* (Figure S4A). Several of these changes were confirmed by qPCR (Figure 5A-B). Using this technique, we also obtained evidence for an increase in *Cxcl10* (p=0.05), a chemokine known to be involved in type 1 diabetes development (Frigerio et al., 2002; Roep et al., 2010) (Figure 5A). The array data revealed also a strong increase in the level of the Eosinophil-associated ribonuclease family members, *Ear1*, *Ear2* and *Ear12* (Table S2). The role of these RNases in β-cells has so far not been explored but, in other cell-types, Ear proteins have cytotoxic and chemoattractant effects (Gupta et al., 2013; Rosenberg, 2015). Interestingly, overexpression of miR-142-3p/-5p and miR-155 in mouse islet cells led to an increase in the level of *Ccl2*, *Ccl7* and *Cxcl10* similar to that observed upon incubation with exoNOD (Figure 5C), indicating that at least part of the effect of the exosomes is mediated by the

transfer of these miRNAs. Exposure of human islets to the exosomes released by activated human $CD4^+$ T cells (exo-hT) led to a similar increase in *CCL2*, *CCL7* and *CXCL10* (Figure 5D), indicating that this phenomenon is not restricted to rodents.

To better understand the cell-specific apoptotic effect of exosomes, we incubated FACS-sorted α- and β-cells with exoNOD for 72h. We found that miRNAs are transferred to both cell types (see Figure 4D-E), but the rise of *Ccl2*, and *Cxcl10* was only observed in β-cells (Figure 5E). A similar trend was observed for *Ccl7*. These results suggest that the selective effect of the exosomes is likely to be caused by the activation of cell-death signaling pathways operating predominantly in β-cells.

Several of the differentially expressed genes are elicited in response to the activation of NFκB, a signaling pathway known to trigger β-cells apoptosis (Melloul, 2008). Consistent with this observation, exposure of MIN6B1 cells to ExoT was associated with a nuclear translocation of NFκB (Figure 5F + Figure S4). The fraction of cells in which NFκB localized in the nucleus after ExoT treatment was very similar to that observed upon exposure to pro-inflammatory cytokines (Figure 5F). Interestingly, the translocation of the transcription factor could be reproduced by directly overexpressing miR-142-3p, miR-142-5p or miR-155 (Figure 5F), confirming a causal link with the transfer of these miRNAs.

Inactivation of miR-142-3p, miR-142-5p and miR-155 prevents exosome-induced cell death.

To determine whether the transferred miRNAs contribute to the deleterious effect of T-cell exosomes on β-cell activities, we directly increased their level using miRNA mimics (Figure S5A,C). While none of the tested miRNAs affected insulin secretion or content (Figure 6A +Figure S5B), overexpression of miR-142-3p, miR-142-5p or miR-155 increased apoptosis both in MIN6B1 (Figure S5D) and rat islet cells (Figure 6B). If the transfer of specific miRNAs from T cells to β-cells contributes to apoptosis induced by exosomes, then inactivation of these miRNAs in receiving cells should prevent cell death. We first verified this hypothesis *in vitro* using anti-miRs that specifically block the action

of the transferred miRNAs. Anti-miRs will not avoid the transfer of the miRNAs but will sequester them upon delivery inside the recipient β-cells, blocking the interaction with their targets. Transfection of islet cells with anti-miR-142-3p, anti-miR-142-5p or anti-hsa-miR-155 attenuated the rise of these non-coding RNAs (Figure S6A-C) and prevented apoptosis induced by exoT (Figure 6C). This effect was specific to exosome-induced apoptosis since these anti-miRs failed to protect β-cells exposed to pro-inflammatory cytokines (Figure S6E-G). While decreasing the level of endogenous miR-155, transfection of rat islet cells with an anti-miR against murine miR-155 did not prevent cell death (Figure 6C and Figure S6D). Taken together, these results suggest that miR-142-3p, miR-142-5p and miR-155 transferred by exosomes from T lymphocytes to β-cells induce recipient cell death.

Injection of a miRNA sponge in 4 weeks old NOD mice prevents T1D development.

Our findings suggest that a transfer of a subset of miRNAs from immune cells to β-cells taking place during the initial phases of T1D could potentially contribute to the development of the disease. To assess the pathophysiological relevance of this exosome-mediated cell-to-cell signaling *in vivo*, we engineered an Adeno Associated Virus (AAV) producing a GFP transcript containing multiple binding sites for miR-142-3p/-5p, miR-150 and miR-155. This "miRNA sponge" is driven by the insulin promoter and specifically sequesters these miRNAs once delivered inside the β-cells (Figure 7A) (Ebert et al., 2007). As at the beginning of our study it was not clear whether miR-150 would be involved in diabetes development, we decided to include in the construct also the binding site of this miRNA. The miRNA sponge or a control AAV lacking the miRNA binding sites were intraperitoneally injected in 4 weeks-old female NOD mice. As expected, GFP mRNA and protein expression was detected in the islet of 8 weeks-old mice injected with the sponge or the control AAV (Figure S7A-B). Importantly, GFP was not detected in the exocrine pancreas and in immune cells invading the islets, confirming the specificity of the insulin promotor (Figure S7C). At 8 weeks of age, both control and sponge-treated NOD mice displayed similar body weights, plasma glucose levels and glucose tolerance

and showed low levels of lymphocyte infiltration (Figure S7D-F + S8A-B). However, while at 32 weeks of age 80% of the control mice became diabetic, only 40% of the animals receiving the miRNA sponge developed the disease (Figure 7B). Histological analysis of the pancreases at the time of sacrifice revealed that these disease-free mice (Sp-prot) retain a higher insulin volume compared to the animals developing diabetes (Figure 7C). Moreover, their islets more often displayed low insulitis scores (Figure 7D). This was not associated with an increase in FoxP3-positive T_{reg} lymphocytes suggesting a decrease in inflammation rather than changes in the cell populations of the immune infiltrate (Figure S8C). Consistent with this hypothesis, we found reduced levels of CXCL10 in islet cells (Figure 7E). In line with our *in vitro* observations, CXCL10 was more frequently found in insulin-positive cells compared to glucagon-positive cells and the expression of this chemokine in β-cells was significantly reduced in sponge-protected mice (Figure 7E). CXCL10 levels were already lower in sponge-treated 8 weeks-old mice compared to control animals suggesting a diminished chemoattractant ability of the β-cells expressing the miRNA sponge (Figure 7F).

Taken together, these *in vivo* data support the relevance of the exosome-mediated transfer of genetic material in the autoimmune reaction and indicate that the inactivation of miR-142-3p/-5p, miR-150 and miR-155 in β-cells is able to protect NOD mice against T1D development.

DISCUSSION

The autoimmune attack of β-cells is a hallmark of T1D, but the events culminating in the specific loss of the insulin-secreting cells remain poorly understood. In the present study, we provide evidence for the involvement of an exosome-mediated transfer of miRNAs from T lymphocytes to β-cells in the initial phases of T1D development. Exosomes have been shown to participate to the etiology of other autoimmune disorders (Robbins et al., 2016; Turpin et al., 2016). Indeed, these small extracellular vesicles can activate specific signal transduction pathways, participate in the formation of immune complexes and synapses, and contribute to the maintenance of the inflammatory status. We observed that exposure of β-cells to exosomes released from T lymphocytes does not alter their secretory capacity but increase their apoptotic rate. An important feature of the autoimmune attack of pancreatic islets is the selective killing of the β-cells. Interestingly, the exosomes released by T cells reproduce this β-cell specific event and have no deleterious impact on α-cells. This cell selectivity cannot be explained by a specific targeting of the exosomes to β-cells, since these small extracellular vesicles are internalized by other islet cell types. β-cell-specific apoptosis is most likely the result of the activation by exosomes of cell death pathways operating only in insulin-secreting cells. Human and rodent α-cells have been reported to be resistant to metabolic and immune stresses that induce β-cell death (Marroqui et al., 2015; Takeda et al., 2012; Vasu et al., 2015). In agreement with this hypothesis, *Ccl2*, *Ccl7* and *Cxcl10* were solely increased in β-cells and not in α-cells upon exosome treatment. Moreover, in NOD mice developing diabetes CXCL10 was more frequently detected in insulin-positive cells than in glucagon-positive cells.

The exosome cargo includes proteins and nucleic acids, in particular miRNAs. We previously identified a subset of miRNAs that are highly abundant in the islets of pre-diabetic NOD mice (Roggli et al., 2012). We show here that this increase cannot be explained by the exposure of β-cells to pro-inflammatory cytokines but is rather the result of an exosome-mediated shuttling of miR-142-3p/-5p and miR-155 from T lymphocytes to β-cells. Our data provide strong evidence indicating that the

transfer of these miRNAs is instrumental to induce β-cell death. Indeed, overexpression of these miRNAs is sufficient to induce β-cell apoptosis and blockade of these miRNAs inside the β-cells prevents apoptosis induced by T-cell exosomes but not by pro-inflammatory cytokines. Individually, none of the predicted targets of the miRNAs is able to explain the activation of NFkB or the observed increase in apoptosis. This is not surprising because miRNAs are known to function by inducing relatively small changes in the expression of a large number of genes rather than by causing major changes in the level of a single transcript. Computational analysis suggests that miR-142-3p, miR-142-5p and miR-155 share some common targets (Table S3), some of which are known to participate to the regulation of cytokine and/or NFκB signaling. Thus, the signaling cascades activated in response to a rise of these miRNAs may potentially converge. Indeed, in agreement with reports in other cell types (Sharma et al., 2012; Yin et al., 2017), miR-142-3p, miR-142-5p and miR-155 were all found to modulate NFκB activity, pointing to a common mode of action. Thus, although the overexpression of each individual miRNA can potentially lead to cell death, the effect of the T cell exosomes is likely to result from the synergistic action of the three miRNAs. In fact, blockade of any of the three transferred miRNAs was sufficient to prevent exosome-induced apoptosis.

We were able to prove the relevance of this novel exosome-mediated cell-to-cell communication mode for T1D development by taking advantage of an AAV construct containing multiple binding sites for miR-142-3p/-5p, miR-150 and miR-155. Indeed, NOD mice injected with this miRNA sponge showed a 50% reduction in the incidence of the disease compared to the control group. As expected, this protection against T1D development was accompanied with a higher islet insulin volume and lower insulitis scores. Whether the protective effect of the miRNA sponge is limited to β-cell death or prevents also the initial steps of the disease remains to be defined. Since an efficient transfer of miRNAs from lymphocytes to β-cells involves the close proximity of the two cells, this event is very unlikely to constitute the initial trigger of the disease. However, once the autoimmune reaction has been initiated by viral antigens, autoantigens or other inflammatory mediators and

immune cells are recruited to the islets, β-cell chemokine production resulting from the transfer of the miRNAs may contribute to maintain and further exacerbate the insulitis. This scenario is consistent with the reduced immune infiltration of the islets observed in mice treated with the miRNA sponge. To precisely define the contribution of exosome-mediated miRNA transfer to the different stages of the diseases, large cross-sectional studies monitoring the impact of the miRNA sponge on insulitis progression and β-cell loss during the natural course of diabetes will be needed.

Interestingly, Ying and colleagues recently demonstrated the detrimental effect of miR-155 released in exosomes from macrophages residing in adipose tissue of obese mice on systemic insulin sensitivity and glucose tolerance. These metabolic markers were improved in miR-155 knockout animals (Ying et al., 2017). Therefore, the release by immune cells of miR-155 in exosomes may possibly be implicated in the etiology of both T1D and T2D.

The precise mechanisms through which the exosomes of T lymphocytes trigger β-cell death remain to be fully established. *In vitro*, activation of NFκB signaling as well as the induction of several members of the Ear family that are cytotoxic in other cell types (Gupta et al., 2013; Rosenberg, 2015) may contribute to the increase in the apoptotic rate observed upon exposure to exosomes. *In vivo*, T lymphocyte exosomes may be part of the mechanisms favoring islet inflammation, insulitis progression and T1D development. Under inflammatory conditions, β-cells are known to produce chemokines such as CCL2 and CXCL10 that are believed to favor insulitis and diabetes development (Frigerio et al., 2002; Martin et al., 2008). The expression of these inflammatory mediators was also observed in pancreatic sections or in islet samples of human T1D donors (Eizirik et al., 2012; Roep et al., 2010). In our study, global expression profiling of mouse islets incubated with exosomes from NOD T effector cells revealed the up-regulation of several genes linked to cytokine and chemokine signaling, including *Ccl2*, *Ccl7*, *Cxcl10* and *Ifng*. Interestingly, Ccl2 was found to modulate NFκB signaling in MIN6 cells (Cai et al., 2011) and other cell types (Viedt et al., 2002; Viedt and Orth, 2002). At least part of these gene expression changes may be driven by the transfer of miRNAs from

immune cells to β-cells. Indeed, overexpression of miR-142-3p, miR-142-5p and miR-155 in β-cells led to an increase in *Ccl2, Ccl7* and *Cxcl10* expression and favored nuclear translocation of NFκB. CXCL10 levels are reduced in β-cells of NOD mice injected with the AAV-sponge and protected from diabetes development. Therefore, *in vivo*, the exposure to exosomes may exacerbate the release of cytokines and chemokines from β-cells elicited in response to inflammatory mediators produced by T lymphocytes, favoring insulitis progression and T1D development.

The exosome-mediated dialogue between lymphocytes and β-cells may operate in both directions. Indeed, these vesicles were reported in other immune diseases to activate T lymphocytes either directly or indirectly via the antigen-presenting cells (Turpin et al., 2016). The release of exosomes from human and rodent islet cells or by insulinoma cell lines has been reported by several laboratories (Bashratyan et al., 2013; Cianciaruso et al., 2017; Guay et al., 2015; Sheng et al., 2011). Sheng and colleagues (Sheng et al., 2011) observed that injection of exosomes produced by MIN6 cells in NOR mice favors lymphocyte islet infiltration and increases insulitis. *In vitro*, exosomes from MIN6 cells were found to trigger both innate and antigen-specific signals by inducing lymphocyte proliferation and by activating autoreactive T-helper 1 cells and marginal zone-like B cells (Bashratyan et al., 2013; Sheng et al., 2011). The precise mechanisms through which β-cell exosomes trigger the immune response remain to be unveiled. Exosomes released by rat and human islet cells contain three autoantigens linked to T1D, namely GAD65, IA-2 and proinsulin, and are taken up by dendritic cells causing their activation (Cianciaruso et al., 2017). The presence of these autoantigens in exosomes released by β-cells could explain how these proteins become the target of the immune system even if they are localized mainly inside the cells. Indeed, exosome-mimetic liposomes transporting GAD65 could favor antigen presentation and T-cell activation. Finally, other components of β-cell exosomes were also involved in stimulation of antigen-presenting cells (Cianciaruso et al., 2017).

In the present study, we focused on miRNAs transferred from $CD4^+$ T effector cells to β-cells. However, other immune cells infiltrating the islets release exosomes with a similar miRNA content.

For example, miR-150 and miR-155 are released in exosomes originating from monocytes and macrophages, respectively, and have functional impacts on recipient cells (Ying et al., 2017; Zhang et al., 2010). The composition of the immune infiltrate and the origin of the exosomes may differ with the progression of the disease. Our data do not exclude the contribution of exosomes produced by other immune cells infiltrating the islets in β-cell dysfunction and loss. We believe that the transfer of miRNAs to β-cells during T1D development is mainly promoted by the close proximity of the activated immune cells that invade the islets. However, the amount and the composition of the exosome cargo varies depending on the activation state of the immune cells (Gutierrez-Vazquez et al., 2013; Okoye et al., 2014; van der Vlist et al., 2012). Indeed, the exosomes released by active T cells were reported to contain higher levels of miR-142-3p (Sukma Dewi et al., 2017). *In vivo*, it is possible that the presence of autoreactive T cell receptors or of other specific components at the exosome surface of infiltrating immune cells may facilitate the fusion with the β-cells and the delivery of the miRNAs. Moreover, the exosomes released by immune cells may carry additional molecules potentially affecting the activity of the target cells, including other RNAs, proteins and lipids. A better understanding of the mechanisms governing the targeting of the exosomes and of the cargo they deliver will not only help elucidating the mechanisms triggering T1D but may also shed new light on the etiology of other autoimmune diseases.

Our findings have relevant implications for the design of better approaches to prevent T1D development. Strategies to avert the loss of β-cells will need to take into account the existence of this newly discovered cell-to-cell signaling mechanism. The exosome-mediated transfer of miRNAs with harmful effects on β-cells is probably exacerbating the deleterious impact of pro-inflammatory cytokines released by the invading immune cells and is likely to synergize with other well-described events involved in the autoimmune reaction. Thus, therapeutic interventions tackling several aspects of the immune attack would probably be more effective in protecting the β-cells.

Limitations of the study

In this study, we showed that a viral construct blocking the activity of a group of miRNAs transferred from lymphocytes to β-cells reduces the incidence of T1D in NOD mice. Although these mice constitute a widely used model of T1D and reproduce many of the feature of the disease in humans (Pearson et al., 2016), additional investigations will be needed to assess the translational potential of our findings. In fact, human T1D is characterized by less pronounced intra-islet infiltration and several immunotherapies preventing the disease in NOD mice were found to be inefficient in humans (Kolb and von Herrath, 2017). Future experiments will also have to investigate the efficacy of the treatment at different stages of the disease. Indeed, in this study the miRNA sponge was injected prior to the initiation of the autoimmune reaction and we ignore whether the treatment would be equally efficient after intra-islet infiltration has occurred. This information will be essential to evaluate the therapeutic potential for human T1D of strategies targeting the exosome-mediated process unveiled in this study.

ACKNOWLEDGEMENTS

We would like to thank Sintia Winkler and Stefanie Siegert from the Flow Cytometry Facility at the Ludwig Center for Cancer Research of the University of Lausanne in Switzerland for FACS sorting and Image Stream analysis, Elizabeth Errazuriz from CIQLE Rockefeller of the University of Lyon in France for Transmission Electron Microscopy images and Alistair Williams, Kyla Chandler and Sian Grace from the University of Bristol for autoantibody measurements. The miR-155 sensor plasmid was kindly provided by Prof. Renne (University of Florida, FL). This work was supported by grants from the Swiss National Science Foundation 31003A-127254 (R.R), European Foundation for the Study of Diabetes (R.R.), Fondation Romande pour la recherche sur le diabète (R.R.), Novartis Foundation for Medical-Biological Research (R.R.), Dutch Diabetes Foundation (J.K.K.), Foundation of the Beatrix Children's Hospital (J.K.K.), Fondation pour la Recherche Médicale FRM-2010 (S.R.), Framework Program 7 from the European Union - Project PEVNET 261441 (F.D.), from the Italian Ministry of Research no. 2015373Z39_007 (F.D.) and from Fondazione Roma (F.D.) and by fellowships from SNF Ambizione PZ00P3_161459 (C.J.), Fonds de Recherche du Québec-santé (C.G.), Canadian Diabetes Association (C.G.) and Société Francophone du Diabète (C.G.).

AUTHOR CONTRIBUTIONS

R.R. conceived the study; C.G., J.K.K. and R.R. designed the experiments; C.G., S.R., V.M., A.D. B.J.G., C.J., K.B. and M.P. carried out *in vitro* experiments and collected the data. J.K.K., N.L.M. and A.J. conducted the *in vivo* experiments on NOD mice and collected the data. F.M. and G.S. performed histological analysis. C.G., J.K.K., S.R., A.D., F.M., G.S., C.B., P.R., F.D. and R.R. contributed to the analysis and interpretation of the data. C.G. and R.R. wrote the manuscript. All authors critically reviewed the manuscript and approved its final version.

DECLARATION OF INTERESTS

The authors declare no competing interests.

REFERENCES

Anderson, M.S., and Bluestone, J.A. (2005). The NOD mouse: a model of immune dysregulation. Annu Rev Immunol 23, 447-485.

Atkinson, M.A., Eisenbarth, G.S., and Michels, A.W. (2014). Type 1 diabetes. Lancet 383, 69-82.

Atkinson, M.A., and Leiter, E.H. (1999). The NOD mouse model of type 1 diabetes: as good as it gets? Nat Med 5, 601-604.

Bashratyan, R., Sheng, H., Regn, D., Rahman, M.J., and Dai, Y.D. (2013). Insulinoma-released exosomes activate autoreactive marginal zone-like B cells that expand endogenously in prediabetic NOD mice. Eur J Immunol 43, 2588-2597.

Bravo-Egana, V., Rosero, S., Klein, D., Jiang, Z., Vargas, N., Tsinoremas, N., Doni, M., Podetta, M., Ricordi, C., Molano, R.D., Pileggi, A., and Pastori, R.L. (2012). Inflammation-Mediated Regulation of MicroRNA Expression in Transplanted Pancreatic Islets. J Transplant 2012, 723614.

Cai, K., Qi, D., Hou, X., Wang, O., Chen, J., Deng, B., Qian, L., Liu, X., and Le, Y. (2011). MCP-1 upregulates amylin expression in murine pancreatic beta cells through ERK/JNK-AP1 and NF-kappaB related signaling pathways independent of CCR2. PLoS One 6, e19559.

Cianciaruso, C., Phelps, E.A., Pasquier, M., Hamelin, R., Demurtas, D., Alibashe Ahmed, M., Piemonti, L., Hirosue, S., Swartz, M.A., De Palma, M., Hubbell, J.A., and Baekkeskov, S. (2017). Primary Human and Rat beta-Cells Release the Intracellular Autoantigens GAD65, IA-2, and Proinsulin in Exosomes Together With Cytokine-Induced Enhancers of Immunity. Diabetes 66, 460-473.

Dudda, J.C., Salaun, B., Ji, Y., Palmer, D.C., Monnot, G.C., Merck, E., Boudousquie, C., Utzschneider, D.T., Escobar, T.M., Perret, R., Muljo, S.A., Hebeisen, M., Rufer, N., Zehn, D., Donda, A., Restifo, N.P., Held, W., Gattinoni, L., and Romero, P. (2013). MicroRNA-155 is required for effector CD8+ T cell responses to virus infection and cancer. Immunity 38, 742-753.

Dumortier, O., Hinault, C., and Van Obberghen, E. (2013). MicroRNAs and metabolism crosstalk in energy homeostasis. Cell Metab 18, 312-324.

Ebert, M.S., Neilson, J.R., and Sharp, P.A. (2007). MicroRNA sponges: competitive inhibitors of small RNAs in mammalian cells. Nat Methods 4, 721-726.

Eizirik, D.L., Colli, M.L., and Ortis, F. (2009). The role of inflammation in insulitis and beta-cell loss in type 1 diabetes. Nat Rev Endocrinol 5, 219-226.

Eizirik, D.L., Sammeth, M., Bouckenooghe, T., Bottu, G., Sisino, G., Igoillo-Esteve, M., Ortis, F., Santin, I., Colli, M.L., Barthson, J., Bouwens, L., Hughes, L., Gregory, L., Lunter, G., Marselli, L., Marchetti, P., McCarthy, M.I., and Cnop, M. (2012). The human pancreatic islet transcriptome:

expression of candidate genes for type 1 diabetes and the impact of pro-inflammatory cytokines. PLoS Genet 8, e1002552.
Eliasson, L., and Esguerra, J.L. (2014). Role of non-coding RNAs in pancreatic beta-cell development and physiology. Acta Physiol (Oxf) 211, 273-284.
Figliolini, F., Cantaluppi, V., De Lena, M., Beltramo, S., Romagnoli, R., Salizzoni, M., Melzi, R., Nano, R., Piemonti, L., Tetta, C., Biancone, L., and Camussi, G. (2014). Isolation, characterization and potential role in beta cell-endothelium cross-talk of extracellular vesicles released from human pancreatic islets. PLoS One 9, e102521.
Filios, S.R., and Shalev, A. (2015). beta-Cell MicroRNAs: Small but Powerful. Diabetes 64, 3631-3644.
Frigerio, S., Junt, T., Lu, B., Gerard, C., Zumsteg, U., Hollander, G.A., and Piali, L. (2002). Beta cells are responsible for CXCR3-mediated T-cell infiltration in insulitis. Nat Med 8, 1414-1420.
Gotoh, M., Maki, T., Satomi, S., Porter, J., Bonner-Weir, S., O'Hara, C.J., and Monaco, A.P. (1987). Reproducible high yield of rat islets by stationary in vitro digestion following pancreatic ductal or portal venous collagenase injection. Transplantation 43, 725-730.
Grieco, F.A., Sebastiani, G., Juan-Mateu, J., Villate, O., Marroqui, L., Ladriere, L., Tugay, K., Regazzi, R., Bugliani, M., Marchetti, P., Dotta, F., and Eizirik, D.L. (2017). MicroRNAs miR-23a-3p, miR-23b-3p, and miR-149-5p Regulate the Expression of Proapoptotic BH3-Only Proteins DP5 and PUMA in Human Pancreatic beta-Cells. Diabetes 66, 100-112.
Guay, C., Menoud, V., Rome, S., and Regazzi, R. (2015). Horizontal transfer of exosomal microRNAs transduce apoptotic signals between pancreatic beta-cells. Cell Commun Signal 13, 17.
Guay, C., and Regazzi, R. (2015). Role of islet microRNAs in diabetes: which model for which question? Diabetologia 58, 456-463.
Guay, C., and Regazzi, R. (2016). New emerging tasks for microRNAs in the control of beta-cell activities. Biochim Biophys Acta 1861, 2121-2129.
Guay, C., Roggli, E., Nesca, V., Jacovetti, C., and Regazzi, R. (2011). Diabetes mellitus, a microRNA-related disease? Transl Res 157, 253-264.
Gupta, S.K., Haigh, B.J., Griffin, F.J., and Wheeler, T.T. (2013). The mammalian secreted RNases: mechanisms of action in host defence. Innate Immun 19, 86-97.
Gutierrez-Vazquez, C., Villarroya-Beltri, C., Mittelbrunn, M., and Sanchez-Madrid, F. (2013). Transfer of extracellular vesicles during immune cell-cell interactions. Immunol Rev 251, 125-142.
Jacovetti, C., Matkovich, S.J., Rodriguez-Trejo, A., Guay, C., and Regazzi, R. (2015). Postnatal beta-cell maturation is associated with islet-specific microRNA changes induced by nutrient shifts at weaning. Nat Commun 6, 8084.

Kluiver, J., Slezak-Prochazka, I., Smigielska-Czepiel, K., Halsema, N., Kroesen, B.J., and van den Berg, A. (2012). Generation of miRNA sponge constructs. Methods 58, 113-117.
Kohler, M., Dare, E., Ali, M.Y., Rajasekaran, S.S., Moede, T., Leibiger, B., Leibiger, I.B., Tibell, A., Juntti-Berggren, L., and Berggren, P.O. (2012). One-step purification of functional human and rat pancreatic alpha cells. Integr Biol (Camb) 4, 209-219.
Kolb, H., and von Herrath, M. (2017). Immunotherapy for Type 1 Diabetes: Why Do Current Protocols Not Halt the Underlying Disease Process? Cell Metab 25, 233-241.
Kosaka, N., Iguchi, H., Yoshioka, Y., Takeshita, F., Matsuki, Y., and Ochiya, T. (2010). Secretory mechanisms and intercellular transfer of microRNAs in living cells. J Biol Chem 285, 17442-17452.
Kroesen, B.J., Teteloshvili, N., Smigielska-Czepiel, K., Brouwer, E., Boots, A.M., van den Berg, A., and Kluiver, J. (2015). Immuno-miRs: critical regulators of T-cell development, function and ageing. Immunology 144, 1-10.
Krogvold, L., Wiberg, A., Edwin, B., Buanes, T., Jahnsen, F.L., Hanssen, K.F., Larsson, E., Korsgren, O., Skog, O., and Dahl-Jorgensen, K. (2016). Insulitis and characterisation of infiltrating T cells in surgical pancreatic tail resections from patients at onset of type 1 diabetes. Diabetologia 59, 492-501.
Lasser, C., Eldh, M., and Lotvall, J. (2012). Isolation and characterization of RNA-containing exosomes. J Vis Exp, e3037.
Lilla, V., Webb, G., Rickenbach, K., Maturana, A., Steiner, D.F., Halban, P.A., and Irminger, J.C. (2003). Differential gene expression in well-regulated and dysregulated pancreatic beta-cell (MIN6) sublines. Endocrinology 144, 1368-1379.
Lundberg, M., Seiron, P., Ingvast, S., Korsgren, O., and Skog, O. (2017). Insulitis in human diabetes: a histological evaluation of donor pancreases. Diabetologia 60, 346-353.
Lynn, F.C., Skewes-Cox, P., Kosaka, Y., McManus, M.T., Harfe, B.D., and German, M.S. (2007). MicroRNA expression is required for pancreatic islet cell genesis in the mouse. Diabetes 56, 2938-2945.
Marroqui, L., Masini, M., Merino, B., Grieco, F.A., Millard, I., Dubois, C., Quesada, I., Marchetti, P., Cnop, M., and Eizirik, D.L. (2015). Pancreatic alpha Cells are Resistant to Metabolic Stress-induced Apoptosis in Type 2 Diabetes. EBioMedicine 2, 378-385.
Martin, A.P., Grisotto, M.G., Canasto-Chibuque, C., Kunkel, S.L., Bromberg, J.S., Furtado, G.C., and Lira, S.A. (2008). Islet expression of M3 uncovers a key role for chemokines in the development and recruitment of diabetogenic cells in NOD mice. Diabetes 57, 387-394.
Matsumoto, Y., Kano, M., Akutsu, Y., Hanari, N., Hoshino, I., Murakami, K., Usui, A., Suito, H., Takahashi, M., Otsuka, R., Xin, H., Komatsu, A., Iida, K., and Matsubara, H. (2016). Quantification

of plasma exosome is a potential prognostic marker for esophageal squamous cell carcinoma. Oncol Rep 36, 2535-2543.
Melloul, D. (2008). Role of NF-kappaB in beta-cell death. Biochem Soc Trans 36, 334-339.
Montecalvo, A., Larregina, A.T., Shufesky, W.J., Stolz, D.B., Sullivan, M.L., Karlsson, J.M., Baty, C.J., Gibson, G.A., Erdos, G., Wang, Z., Milosevic, J., Tkacheva, O.A., Divito, S.J., Jordan, R., Lyons-Weiler, J., Watkins, S.C., and Morelli, A.E. (2012). Mechanism of transfer of functional microRNAs between mouse dendritic cells via exosomes. Blood 119, 756-766.
Nathwani, A.C., Gray, J.T., Ng, C.Y., Zhou, J., Spence, Y., Waddington, S.N., Tuddenham, E.G., Kemball-Cook, G., McIntosh, J., Boon-Spijker, M., Mertens, K., and Davidoff, A.M. (2006). Self-complementary adeno-associated virus vectors containing a novel liver-specific human factor IX expression cassette enable highly efficient transduction of murine and nonhuman primate liver. Blood 107, 2653-2661.
Nesca, V., Guay, C., Jacovetti, C., Menoud, V., Peyot, M.L., Laybutt, D.R., Prentki, M., and Regazzi, R. (2013). Identification of particular groups of microRNAs that positively or negatively impact on beta cell function in obese models of type 2 diabetes. Diabetologia 56, 2203-2212.
Okoye, I.S., Coomes, S.M., Pelly, V.S., Czieso, S., Papayannopoulos, V., Tolmachova, T., Seabra, M.C., and Wilson, M.S. (2014). MicroRNA-Containing T-Regulatory-Cell-Derived Exosomes Suppress Pathogenic T Helper 1 Cells. Immunity 41, 503.
Parnaud, G., Bosco, D., Berney, T., Pattou, F., Kerr-Conte, J., Donath, M.Y., Bruun, C., Mandrup-Poulsen, T., Billestrup, N., and Halban, P.A. (2008). Proliferation of sorted human and rat beta cells. Diabetologia 51, 91-100.
Pearson, J.A., Wong, F.S., and Wen, L. (2016). The importance of the Non Obese Diabetic (NOD) mouse model in autoimmune diabetes. J Autoimmun 66, 76-88.
Rebeaud, F., Hailfinger, S., Posevitz-Fejfar, A., Tapernoux, M., Moser, R., Rueda, D., Gaide, O., Guzzardi, M., Iancu, E.M., Rufer, N., Fasel, N., and Thome, M. (2008). The proteolytic activity of the paracaspase MALT1 is key in T cell activation. Nat Immunol 9, 272-281.
Reed, S.E., Staley, E.M., Mayginnes, J.P., Pintel, D.J., and Tullis, G.E. (2006). Transfection of mammalian cells using linear polyethylenimine is a simple and effective means of producing recombinant adeno-associated virus vectors. J Virol Methods 138, 85-98.
Ridder, K., Keller, S., Dams, M., Rupp, A.K., Schlaudraff, J., Del Turco, D., Starmann, J., Macas, J., Karpova, D., Devraj, K., Depboylu, C., Landfried, B., Arnold, B., Plate, K.H., Hoglinger, G., Sultmann, H., Altevogt, P., and Momma, S. (2014). Extracellular vesicle-mediated transfer of genetic information between the hematopoietic system and the brain in response to inflammation. PLoS Biol 12, e1001874.

Robbins, P.D., Dorronsoro, A., and Booker, C.N. (2016). Regulation of chronic inflammatory and immune processes by extracellular vesicles. J Clin Invest 126, 1173-1180.
Roep, B.O., Kleijwegt, F.S., van Halteren, A.G., Bonato, V., Boggi, U., Vendrame, F., Marchetti, P., and Dotta, F. (2010). Islet inflammation and CXCL10 in recent-onset type 1 diabetes. Clin Exp Immunol 159, 338-343.
Roggli, E., Gattesco, S., Caille, D., Briet, C., Boitard, C., Meda, P., and Regazzi, R. (2012). Changes in microRNA expression contribute to pancreatic beta-cell dysfunction in prediabetic NOD mice. Diabetes 61, 1742-1751.
Rosenberg, H.F. (2015). Eosinophil-Derived Neurotoxin (EDN/RNase 2) and the Mouse Eosinophil-Associated RNases (mEars): Expanding Roles in Promoting Host Defense. Int J Mol Sci 16, 15442-15455.
Sharma, S., Liu, J., Wei, J., Yuan, H., Zhang, T., and Bishopric, N.H. (2012). Repression of miR-142 by p300 and MAPK is required for survival signalling via gp130 during adaptive hypertrophy. EMBO Mol Med 4, 617-632.
Sheng, H., Hassanali, S., Nugent, C., Wen, L., Hamilton-Williams, E., Dias, P., and Dai, Y.D. (2011). Insulinoma-released exosomes or microparticles are immunostimulatory and can activate autoreactive T cells spontaneously developed in nonobese diabetic mice. J Immunol 187, 1591-1600.
Skalsky, R.L., Samols, M.A., Plaisance, K.B., Boss, I.W., Riva, A., Lopez, M.C., Baker, H.V., and Renne, R. (2007). Kaposi's sarcoma-associated herpesvirus encodes an ortholog of miR-155. J Virol 81, 12836-12845.
Soo, C.Y., Song, Y., Zheng, Y., Campbell, E.C., Riches, A.C., Gunn-Moore, F., and Powis, S.J. (2012). Nanoparticle tracking analysis monitors microvesicle and exosome secretion from immune cells. Immunology 136, 192-197.
Sukma Dewi, I., Celik, S., Karlsson, A., Hollander, Z., Lam, K., McManus, J.W., Tebbutt, S., Ng, R., Keown, P., McMaster, R., McManus, B., Ohman, J., and Gidlof, O. (2017). Exosomal miR-142-3p is increased during cardiac allograft rejection and augments vascular permeability through down-regulation of endothelial RAB11FIP2 expression. Cardiovasc Res 113, 440-452.
Takeda, Y., Fujita, Y., Honjo, J., Yanagimachi, T., Sakagami, H., Takiyama, Y., Makino, Y., Abiko, A., Kieffer, T.J., and Haneda, M. (2012). Reduction of both beta cell death and alpha cell proliferation by dipeptidyl peptidase-4 inhibition in a streptozotocin-induced model of diabetes in mice. Diabetologia 55, 404-412.
Thery, C., Ostrowski, M., and Segura, E. (2009). Membrane vesicles as conveyors of immune responses. Nat Rev Immunol 9, 581-593.

Thomou, T., Mori, M.A., Dreyfuss, J.M., Konishi, M., Sakaguchi, M., Wolfrum, C., Rao, T.N., Winnay, J.N., Garcia-Martin, R., Grinspoon, S.K., Gorden, P., and Kahn, C.R. (2017). Adipose-derived circulating miRNAs regulate gene expression in other tissues. Nature 542, 450-455.
Tugay, K., Guay, C., Marques, A.C., Allagnat, F., Locke, J.M., Harries, L.W., Rutter, G.A., and Regazzi, R. (2016). Role of microRNAs in the age-associated decline of pancreatic beta cell function in rat islets. Diabetologia 59, 161-169.
Turpin, D., Truchetet, M.E., Faustin, B., Augusto, J.F., Contin-Bordes, C., Brisson, A., Blanco, P., and Duffau, P. (2016). Role of extracellular vesicles in autoimmune diseases. Autoimmun Rev 15, 174-183.
Valadi, H., Ekstrom, K., Bossios, A., Sjostrand, M., Lee, J.J., and Lotvall, J.O. (2007). Exosome-mediated transfer of mRNAs and microRNAs is a novel mechanism of genetic exchange between cells. Nat Cell Biol 9, 654-659.
van der Vlist, E.J., Nolte-'t Hoen, E.N., Stoorvogel, W., Arkesteijn, G.J., and Wauben, M.H. (2012). Fluorescent labeling of nano-sized vesicles released by cells and subsequent quantitative and qualitative analysis by high-resolution flow cytometry. Nat Protoc 7, 1311-1326.
Vasu, S., Moffett, R.C., McClenaghan, N.H., and Flatt, P.R. (2015). Differential molecular and cellular responses of GLP-1 secreting L-cells and pancreatic alpha cells to glucotoxicity and lipotoxicity. Exp Cell Res 336, 100-108.
Viedt, C., Dechend, R., Fei, J., Hansch, G.M., Kreuzer, J., and Orth, S.R. (2002). MCP-1 induces inflammatory activation of human tubular epithelial cells: involvement of the transcription factors, nuclear factor-kappaB and activating protein-1. J Am Soc Nephrol 13, 1534-1547.
Viedt, C., and Orth, S.R. (2002). Monocyte chemoattractant protein-1 (MCP-1) in the kidney: does it more than simply attract monocytes? Nephrol Dial Transplant 17, 2043-2047.
Weber, J.A., Baxter, D.H., Zhang, S., Huang, D.Y., Huang, K.H., Lee, M.J., Galas, D.J., and Wang, K. (2010). The microRNA spectrum in 12 body fluids. Clin Chem 56, 1733-1741.
Wu, H., Neilson, J.R., Kumar, P., Manocha, M., Shankar, P., Sharp, P.A., and Manjunath, N. (2007). miRNA profiling of naive, effector and memory CD8 T cells. PLoS One 2, e1020.
Yin, H., Song, S., and Pan, X. (2017). Knockdown of miR-155 protects microglia against LPS-induced inflammatory injury via targeting RACK1: a novel research for intracranial infection. J Inflamm (Lond) 14, 17.
Ying, W., Riopel, M., Bandyopadhyay, G., Dong, Y., Birmingham, A., Seo, J.B., Ofrecio, J.M., Wollam, J., Hernandez-Carretero, A., Fu, W., Li, P., and Olefsky, J.M. (2017). Adipose Tissue Macrophage-Derived Exosomal miRNAs Can Modulate In Vivo and In Vitro Insulin Sensitivity. Cell 171, 372-384 e312.

Zhang, L., Zhang, S., Yao, J., Lowery, F.J., Zhang, Q., Huang, W.C., Li, P., Li, M., Wang, X., Zhang, C., Wang, H., Ellis, K., Cheerathodi, M., McCarty, J.H., Palmieri, D., Saunus, J., Lakhani, S., Huang, S., Sahin, A.A., Aldape, K.D., Steeg, P.S., and Yu, D. (2015). Microenvironment-induced PTEN loss by exosomal microRNA primes brain metastasis outgrowth. Nature 527, 100-104.

Zhang, Y., Liu, D., Chen, X., Li, J., Li, L., Bian, Z., Sun, F., Lu, J., Yin, Y., Cai, X., Sun, Q., Wang, K., Ba, Y., Wang, Q., Wang, D., Yang, J., Liu, P., Xu, T., Yan, Q., Zhang, J., Zen, K., and Zhang, C.Y. (2010). Secreted monocytic miR-150 enhances targeted endothelial cell migration. Mol Cell 39, 133-144.

Zolotukhin, S., Byrne, B.J., Mason, E., Zolotukhin, I., Potter, M., Chesnut, K., Summerford, C., Samulski, R.J., and Muzyczka, N. (1999). Recombinant adeno-associated virus purification using novel methods improves infectious titer and yield. Gene Ther 6, 973-985.

Zomer, A., Maynard, C., Verweij, F.J., Kamermans, A., Schafer, R., Beerling, E., Schiffelers, R.M., de Wit, E., Berenguer, J., Ellenbroek, S.I., Wurdinger, T., Pegtel, D.M., and van Rheenen, J. (2015). In Vivo imaging reveals extracellular vesicle-mediated phenocopying of metastatic behavior. Cell 161, 1046-1057.

FIGURE LEGENDS

Figure 1 - Deregulation of miRNA levels in β-cells of prediabetic NOD mice A) Abundance of the indicated miRNAs in A) islets of diabetes-free SCID-NOD mice (n=3 indep. exp.) or B) in FACS-sorted β-cells of NOD mice (n=4 indep. exp.) aged of 4 and 8 weeks. C) Islets of control C57Bl/6N mice were incubated in the presence of pro-inflammatory cytokines (IFNγ, TNFα and IL-1β) (n=6 indep. exp.). miRNA levels were determined by qPCR and are expressed as fold change vs 4 weeks or control (Ctl) condition (white bars). miR-146a was used as a positive control for cytokine treatment. * $p < 0.05$, ** $p < 0.01$ by Student's t-test. See also Figure S1.

Figure 2 - Characterization of the exosomes released by T lymphocytes. Exosomes were isolated from the culture media of Jurkat cells (exoT) or NOD T lymphocytes (exoNOD) by sequential centrifugation. A-B) Visualization of the extracellular vesicles (arrows) by electron microscopy (scale bar = 100nm). C) Analysis of the presence of the exosomal markers Alix, CD81 and Tsg101 by western blotting in our extracellular vesicle preparations. The supernatant surrounding the exosome pellet after ultra-centrifugation was used as negative control (Neg. Ctl). Analysis of the size distribution of D) ExoT and E) ExoNOD vesicles using the Nanosight technology. F) Image stream flow cytometry analysis of MIN6B1 cells incubated with DiD-labelled ExoT (4 representative pictures out of 20'171 cells analyzed). Scale bar = 7µm. G) miRNA levels in exoT. A miR-29a mimic, used as positive control for RNAse digestion, was spiked in the ExoT preparation. The samples were then treated or not (NT) with Triton X-100 (T) and incubated with RNAses (+R). miRNA levels were measured by qPCR and are expressed as percentage of NT (n=3 indep. exp).

Figure 3 - T cell exosomes transfer miRNAs to β-cells and induce their death. A) Schematic representation of the in vitro exosome transfer experiments. CD4+CD25- T lymphocytes were isolated from mouse spleen (or alternatively from human blood samples) and cultured for 72h in the presence

of CD3CD28 activation beads, IL-2 and IL-12. Exosomes were isolated from the culture media by ultra-centrifugation and added to recipient islet cells. Mouse islet cells (B,H) were incubated with exoNOD, rat islet cells (C-D,F-G) with exoT and human islet cells (I-K) with exo-hT (n=4-5 indep. exp.) for 48-72h. At the end of the incubation, miRNA abundance was measured by qPCR and was expressed as Fold changes vs Ctl (B-C, I) or as RFU if the miRNA was undetectable under control condition (D). E) Luciferase activity was measured in MIN6B1 cells transfected with the hsa-miR-155 sensor and treated with exoT for 48h or 72h (arbitrary unit AU). F-H, J) Apoptosis was assessed by scoring the cells displaying pycnotic nuclei upon Hoechst staining without or with the pan-caspase inhibitor zVAD, or (K) using TUNEL assay. *,# $p < 0.05$, **,## $p < 0.01$ by Student's t-test or by one-way Anova, Dunnett's post-hoc test for multiple comparison. See also Figure S2-S3 and Table S1.

Figure 4 - T cell exosomes induce specifically β-cell death. FACS-sorted rat islet fractions enriched for (A) β- or (B) α-cells were incubated with exoT for 72h. Apoptosis was assessed by scoring the cells displaying pycnotic nuclei upon Hoechst staining (A: n=5, B: n=3 indep. exp.). C) Analysis by Image stream flow cytometry of rat islet cells incubated with DiD-exoT. Two representative images out of 10'089 cells analyzed. FACS-sorted rat islet fractions enriched for β- (D) or α-cells (E) were incubated with exoNOD for 72h. miRNA levels were measured by qPCR and are expressed as Fold changes vs Ctl (n=3 indep. exp) * $p < 0.05$, ** $p < 0.01$ by Student's t-test.

Figure 5 - Regulation of β-cell gene expression by T cell exosomes. A-B) Confirmation by qPCR of gene expression changes observed by global microarray profiling of mouse islet cells incubated with exoNOD. C-E) Gene expression levels were measured by qPCR in C) dispersed mouse islet cells transfected with miR-142-3p, miR-142-5p and miR-155 mimics, D) human islet cells incubated with exo-hT and E) FACS-sorted rat islet fractions enriched for α- or β-cells incubated with exoNOD. The results are expressed as Fold changes (A, C, D, E) or as relative fluorescent units (RFU) (B), Ifng

being not detected under control condition (n=4 indep. exp.). F) Nuclear translocation of NFκB in MIN6B1 cells incubated with exoT or pro-inflammatory cytokines (IFNγ, TNFα and IL-1β), or transfected with miR-142-3p, miR-142-5p and miR-155 mimics (n=3-4 indep. exp.). * $p < 0.05$, ** $p < 0.01$ Student's t-test. See also Figure S4 and Table S2.

Figure 6 - Effects of miR-142-3p/-5p and miR-155 deregulation on β-cell function and survival. A-B) Dispersed rat islet cells were transfected with the indicated miRNA mimics. A) Insulin secretion in response to 2 or 20 mM glucose (2G or 20G) was measured by ELISA (n=3-6 indep. exp.). B) Apoptosis was assessed by Hoechst staining (n=4 indep. exp.). Cytokine mix (Cyt) was used as positive control. * $p < 0.05$, ** $p < 0.01$ by Student's t-test. C) Dispersed rat islet cells were transfected with the indicated antimiR and incubated with exoT for 72h. At the end of the incubation period, apoptosis was determined by scoring the cells displaying pycnotic nuclei upon Hoechst staining (n=4 indep. exp.). *, # $p < 0.05$. **, ## $p < 0.01$ by one-way Anova, Dunnett's post-hoc test. See also Figure S5 and S6.

Figure 7 - Inactivation of miR-142-3p/-5p, miR-150 and miR-155 in β-cells of NOD mice reduces the incidence of T1D. A) Schematic representation of the AAV producing a GFP transcript containing multiple binding sites for miR-142-3p/-5p, miR-150 and miR-155 (miRNA sponge) driven by the insulin promotor (RIP). The AAV-sponge (Sp) or a control AAV lacking the miRNA binding sites (Ctl) were injected intraperitoneally in NOD mice aged of 4 weeks. B) Diabetes-free animals displaying a glycemia below 14 mM, in the group of mice injected with the AAV-sponge and with AAV-ctl. Total of n=15-16 mice, 3 independent experiments, p=0,0267, by log-rank test. C) Insulin volume determined by immunostaining in AAV-sponge injected animals that developed diabetes (Sp-not protected) or remained disease-free (Sp-protected) until 32 weeks of age (n=70 pancreatic sections, from 3 different mice per group). ** $p < 0.01$ by Mann-Whitney U test. D) Insulitis score measured at

the time of sacrifice in the pancreases of AAV-sponge injected mice that were protected (Sp-prot) or not (Sp-NP) from diabetes development (n=3 mice per group). E) Colocalization of CXCL10 (Red) with insulin- (Green, yellow arrows) or Glucagon- (Blue, red arrows) in 32 weeks old NOD mice injected with the AAV-sponge developing (SP-NP) or not (SP-prot.) diabetes. F) CXCL10 levels (Red) normalized to islet insulin volume (Green) in 8 weeks old NOD mice injected with AAV-Ctl (Ctl) or AAV-sponge (Sp). Nuclei were stained with Dapi (blue) (E) n=35, and (F) n=180 pancreatic sections, from 3 different mice per group. ** $p < 0.01$ by Mann-Whitney U test or by one-way Anova, Tukey's post-hoc test. See also Figure S7-S8.

CONTACT FOR REAGENT AND RESOURCE SHARING

Further information and requests for resources and reagents should be directed to and will be fulfilled by the Lead Contact, Dr. Romano Regazzi (romano.regazzi@unil.ch).

EXPERIMENTAL MODEL AND SUBJECT DETAILS

Rodent **-** All animal procedures were performed in accordance with the NIH guidelines and protocols were approved by the Swiss Research Councils and Veterinary Offices or the Ethical Committee for Animal Experiments of the University of Groningen. Male Wistar rats (200-250g) and 4-8 weeks old female NOD/ShiLtJ mice were obtained from Charles River Laboratories (L'arbresle, France). Male C57Bl/6N mice (12-15 week-old) and 4 and 8 weeks-old female NOD scid mice (NOD.CB17-Prkdcscid/Rj) were from Janvier Labs (Le Genest St-Isle, France). miR-155 knock-out mice (miR-155-/-) were from Jackson Laboratories (Jax 007745).

Human islets - Human islet preparation were obtained from Tetu-Bio (Lot HP-18157-01, Germany) or from the Centre d'Etude Européen pour le Diabète in Strasbourg (isolation protocol authorization for scientific research #PFS12-0013). Dissociated islet cells were cultured in CMRL medium (Invitrogen) supplemented with 10% fetal calf serum (Gibco), 10 mM Hepes pH 7.4, 100 μg/mL streptomycin and 100 IU/mL penicillin and 2 mmol/l glutamine. Detailed information about human islet donors are provided in Table S4 and in Key Resources Tables.

Cell lines **–**Jurkat cells (J77 clone 20 from O. Acuto) (Rebeaud et al., 2008) were cultured in RPMI 1640 medium supplemented with 10% fetal calf serum (previously depleted from serum-exosomes), 50 μg/mL streptomycin and 50 IU/mL penicillin at densities comprised between 0.2 and 1 x 10^6 cells/ml. Jurkat culture media was collected each two to three days for exosome isolation. MIN6B1 cells, a murine insulin-secreting cell line (Lilla et al., 2003), were cultured at a density of 1.5 x 10^5 cells/cm^2 in DMEM-GlutaMAX^{TM} medium (Invitrogen) containing 25 mM glucose and 4 mM L-glutamine, and supplemented with 15% fetal calf serum, 70 μM β-mercaptoethanol, 50 μg/mL

streptomycin and 50 IU/mL penicillin. All cell lines were cultured at 37°C in a humidified atmosphere (5% CO_2, 95% air) and tested negative for mycoplasma contamination.

METHOD DETAILS

Isolation of rodent pancreatic islet cells – Rodent islets were isolated by collagenase digestion of the pancreas (Gotoh et al., 1987) followed by Histopaque density gradient to separate them from digested exocrine tissue. At the end of the isolation, islets were hand-picked and incubated overnight at 37°C in RPMI 1640- GlutaMAX^{TM} medium (Invitrogen) containing 11.1 mM glucose and 2.06 mM L-glutamine and supplemented with 10% fetal calf serum (Gibco), 10 mM Hepes, pH 7.4, 1 mM sodium pyruvate, 100 µg/mL streptomycin and 100 IU/mL penicillin. Dissociated islet cells were obtained by incubating the islets in Ca^{2+}/Mg^{2+} free phosphate buffered saline, 3 mM EGTA and 0.002% trypsin for 5 min at 37°C. For some experiments, rat islet cells were separated by Fluorescence-Activated Cell Sorting (FACS) based on β-cell autofluorescence, as previously described (Jacovetti et al., 2015; Kohler et al., 2012). Sorted islet cells were seeded on plastic dishes coated with extracellular matrix secreted by 804 G rat bladder cancer cells (804 G ECM), as described elsewhere (Parnaud et al., 2008). Enrichment of α - and β-cells was evaluated by double immunofluorescence staining using polyclonal guinea pig anti-insulin (dilution 1:100, A0564, Dako) and polyclonal mouse anti-glucagon (dilution 1:1000, Abcam Ab10988) primary antibodies and goat anti-guinea pig Alexa-Fluor-488 and goat anti-mouse Alexa-Fluor-555 (diluted 1:500, Molecular Probes, Thermofisher A11073 and A21422, respectively) secondary antibodies. On average, β-cell fractions contained 98.1 ± 2.2% insulin-positive cells and 1.4 ± 1.5% glucagon-positive cells and α-cell-enriched fractions contained 5.2 ± 3.5% insulin-positive cells and 91.2 ± 4.3% glucagon-positive cells.

T lymphocyte isolation and culture – Mouse T effector cells were purified from lymphoid tissues of 8 weeks-old NOD/ShiLtJ mice, or miR-155KO mice (or wild type control littermates) using anti-CD4 and anti-CD25 coated beads (Miltenyi Biotec). Human $CD4^+$ T cells were obtained from 3 anonymous

donors that gave informed consent in accordance with the US National Institutes of Health guidelines. Briefly, buffy coats were purchased from the Blood Transfusion Center in Lausanne, Switzerland. Peripheral blood mononuclear cells were isolated by density centrifugation over a Ficoll-Hypaque gradient (Amersham Bioscience) and washed three times. $CD4^+$ T cells were enriched from purified mononuclear cells by positive selection using anti-CD4 magnetic microbeads (Miltenyi Biotec). After isolation, murine $CD4^+/CD25^-$ T cells and human $CD4^+$ T cells were incubated in RPMI 1640-medium supplemented with 10% fetal calf serum (previously depleted from serum-exosomes), 100 µg/mL streptomycin and 100 IU/mL penicillin and were stimulated for 72h with 20 ng/ml IL-12 and 200 UI/ml IL-2 (R&D system Europe) and Dynabeads T-activator CD3/CD28 (bead-to-cell ratio of 1) (Invitrogen). After three days, media and cells were collected for exosome isolation and/or RNA extraction.

Exosome isolation and quantification – Exosomes were isolated by ultra-centrifugation as described previously (Lasser et al., 2012). Briefly, the culture media (depleted from serum-exosomes) of Jurkat cells or primary T cells were collected and centrifuged first at 300 x *g* for 3 min to pellet cells and then at 2000 x *g* for 10 min to discard dead cells. Supernatants were centrifuged at 10'000 x *g* for 30 min to remove cell debris. Exosomes were then isolated from the supernatant by ultracentrifugation at 100'000 x *g* for 2h. The pellet containing the exosomes was washed with PBS and re-centrifuged at 100'000 x *g* for 2h. Exosomes were collected in a minimal volume of PBS. The same volume of PBS (without exosomes) was added to control experimental conditions. Protein concentration was determined by Bradford assay (BioRad). Recipient MIN6B1 or islet cells were incubated with 50 µg/ml of exosome preparation previously passed on a 0.45 µm filter (Figliolini et al., 2014; Guay et al., 2015). The amount of vesicles added to the recipient cells was estimated using the FluoroCet exosome quantification kit (System Biosciences), which is based on the measurement of the esterase activity associated with exosomes. According to these measurements, the recipient cells were exposed to exosome concentrations of about $0.8x10^{11}$/ml for exoT, $0.7x10^{11}$/ml for exoNOD and $2\ x10^{11}$/ml for

exo-hT. These concentrations are within the same range as those previously reported in murine and human plasma samples (Matsumoto et al., 2016; Thomou et al., 2017).

Electron microscopy – Suspensions were adsorbed on 200 Mesh Cupper grids coated with forvmar-C for 2 min at RT. The grids were then stained using 2% phosphotungstic acid for 2 min and observed on a transmission electron microscope (Jeol 1400 JEM, Tokyo, Japan) equipped with a Gatan camera (Orius 600) and Digital Micrograph Software.

Nanosight analysis – Exosome size distribution was measured by Nanoparticle Tracking Analysis using the NanoSight system (NanoSight, UK). The device measures the Brownian motion of particles whose speed of motion, or diffusion coefficient (Dt), is related to particle size through the Stokes-Einstein equation (Soo et al., 2012).

Western blot – Proteins from exosome samples or from cellular lysates were migrated on 10% SDS-PAGE gels. Following electrophoresis, proteins were transferred onto PVDF membranes and blocked at room temperature in Tris-buffered saline/0.3% Tween20 containing 4% of BSA. The membranes were then incubated overnight at 4 °C with CD81 (sc-166028), Alix (sc-49268) or TSG101 (sc-6037) antibodies (Santa Cruz Biotechnology) diluted 1/1000 in 1% BSA. The bands were detected by chemiluminescence (Pierce) after incubation with a horseradish peroxidase-conjugated secondary antibody (Bio-Rad).

Image stream analysis – Exosomes from Jurkat cells were labelled with 1µM of the lipophilic dye DiD (1,1'-dioctadecyl-3,3,3',3'-tetramethylindodicarbocyanine, 4-chlorobenzenesulfonate salt, Molecular Probes) during the last ultracentrifugation (2h at 100’000 x *g*). The labelled-exosome pellet was washed twice in PBS before another round of ultracentrifugation (2h at 100’000 *g*). MIN6B1 cells or dissociated rat islet cells were incubated overnight in the presence of DiD-labelled exoT, before being analyzed on Amnis ImageStream^X Mark II (Merk Millipore).

RNase treatment – Exosome preparations were re-suspended in 300 µl PBS and spiked with 20 ρmol of a synthetic oligonucleotide corresponding to the mature sequence of miR-29a (Exiqon). Samples

were then divided into four aliquots and treated or not with 1% Triton X-100 (Sigma) and incubated with or without RNase A (0.5 U) and RNase T1 (15 U) (Ambion) for 30 min at 37°C before RNA extraction.

RNA assays – RNA was extracted from exosomes, Jurkat, MIN6B1 or islet cells using the miRNeasy micro kit (Qiagen). Mature miRNA levels were measured using the miRCURY LNA^{TM} Universal RT microRNA PCR kit (Exiqon) starting from 200 ng of RNA. Cellular miRNA levels were normalized to miR-7 levels, a miRNA highly expressed in β-cells and not modified under the studied conditions. For mRNA measurement, RNA samples were treated with DNase prior to analysis. Profiling of mRNA was performed by Arraystar (MD, USA) using Agilent Technologies and Agilent GeneSpring GX v12.1 software for data analysis. Gene expression levels were measured by qPCR using miScript II RT and SYBR Green PCR kits (Qiagen) and results were normalized to *18S* rRNA and *Hprt*. Finally, GFP levels were assessed using SYBR Green PCR Master Mix (Life Technologies) with primers specific for GFP and normalized to *Gapdh* levels. Primer sequences are provided in Table S5. All qPCR measurements were performed in triplicates and expression levels of miRNAs and mRNAs were analyzed using the $2^{-\Delta\Delta C(T)}$ method.

Transfection of insulin-secreting cells – MIN6B1 or dispersed rat islet cells were transfected using Lipofectamine 2000^{TM} (Invitrogen) with RNA oligonucleotide duplexes (Exiqon) corresponding to the mature miRNA sequence (overexpression) or with single-stranded miRCURY LNA inhibitors (Exiqon) that specifically block the miRNAs (down-regulation). A control miRNA mimic or the control miRCURY LNA inhibitor (Exiqon) were used as negative controls for miRNA overexpression and down-regulation, respectively.

Insulin secretion and content – After incubation for 72h in the presence of exosomes (or control PBS), MIN6B1 or dissociated rat islet cells were pre-incubated for 30 min at 37°C in Krebs-Ringer bicarbonate buffer (KRBH) containing 25 mM HEPES, pH 7.4, 0.1 % BSA (Sigma-Aldrich) and 2 mM glucose. The cells were then incubated for 45 min in KRBH containing 0.5% BSA and 2 or 20

mM glucose. At the end of the incubation period, media were collected and total cellular insulin contents recovered in acid-ethanol (0.2 mM HCl in 75% ethanol). Insulin levels were measured using an insulin enzyme immunoassay kit (SPI-Bio). All experiments were performed in triplicates.

Cell death assays – MIN6B1 and dissociated islet cells were incubated for 72h in presence of T cell exosomes with or without 0.1mM of the pan caspase inhibitor Z-VAD-FMK (R&D systems). At the end of the incubation, 1 μg/ml Hoechst 33342 (Invitrogen) was added for 1-2 min. Cells displaying pycnotic nuclei were scored under fluorescence microscopy (AxioCam MRc5, Zeiss). A minimum of thousand cells were counted per condition. TUNEL staining on human β-cells was performed 48h after exposure to exo-hT using the In Situ Cell Death Detection Kit (Roche) combined to FLEX polyclonal guinea pig anti-insulin (dilution 1:10, IR00261-2, Dako) followed by incubation with fluorescently-labeled goat anti-guinea-pig AlexaFluor 555 antibody (dilution 1:400, A21435, Thermofisher). NFκB translocation was assessed in MIN6B1 cells after exposure for 48h to exoT or for 24h to pro-inflammatory cytokines (30 ng/ml INFγ, 10 ng/ml TNFα and 0.1 ng/ml IL-1β). Briefly, MIN6B1 cells cultured on coverslips were fixed, permeabilized and incubated with a mouse anti-NFκB p65 antibody (dilution 1:100, sc-372, Santa Cruz Biotechnology) followed by goat anti-mouse Alexa Fluor 488 antibody (A-11029, Invitrogen). Cell nuclei were stained with Hoechst 33342 (1 μg/ml, Invitrogen). Coverslips were mounted on microscope glass slides with Fluor-Save mounting medium (VWR International SA) and were visualized with a Zeiss Axiovision fluorescence microscope. Experiments were performed in single replicates.

Luciferase – MIN6B1 cells were transfected using Lipofectamine 2000^{TM} (Invitrogen) with a pGL3 plasmid containing the hsa-miR-155 binding sequence in the 3'UTR (Skalsky et al., 2007) and the psicheck1 vector (Promega). After 7h, culture media of transfected MIN6B1 was changed and exoT was added for 48h or 72h. Luciferase activities were measured using the Dual-Luciferase Reporter Assay System (Promega). Firefly luciferase activity was normalized to Renilla luciferase activity to minimize experimental variabilities. Experiments were performed in triplicates.

Generation of viral vectors – The dsAAV-RIP-GFP (AAV-control) was constructed on the backbone of the dsAAV8 plasmid (Nathwani et al., 2006) by replacing the original LP1 promotor and FIX coding sequences with two multiple cloning sites and inserting the coding sequences for the Rat Insulin promotor (RIP) (Addgene plasmid 15029) and green fluorescent protein (GFP) into the multiple cloning site, using the PstI-AccIII and EcoRI-NotI restriction sites. For the construction of the dsAAV-RIP-GFP-sponge (AAV-sponge), the interrupted palindromic SanDI (Fermentas) restriction site was used to insert miRNA binding sites for miR-142-3p/-5p, miR-150 and miR-155 (Table S6) (Kluiver et al., 2012). Viral particles were generated by a triple transfection of HEK293 cells using the 25 kDa linear polyethylenimine (Polysciences Inc) transfection method (Reed et al., 2006). AAV particles were purified by iodixanol gradient centrifugation as previous described (Zolotukhin et al., 1999). Viral titers were determined by qPCR with specific primers for the RIP and GFP.

In vivo experiments – Female NOD/ShiLtJ mice were injected intraperitoneally (I.P.) with 150 µl PBS containing 1 $x10^{12}$ viral genome particles at the age of 4 weeks. Blood glucose levels were measured once per week on restrained, un-anesthetized animals through tail vein bleeds with a glucometer and test strips (Life Scan). NOD mice were diagnosed as diabetic if blood glucose levels above 14 mM on 2 consecutive days. Glucose tolerance test was performed by injecting I.P. 1.5g glucose per kg of body weight on 4 hour fasted NOD mice of 10 weeks of age, from the diabetes incidence cohort. Experiments were not performed blinded. One mouse from the AAV-ctl group was excluded and euthanized at 13 days after injection as it met ethical endpoints (loss of more than 15% of body weight after injection and showed signs of discomfort).

Histology and immunohistochemistry – Formalin-fixed pancreatic tissues were embedded in paraffin using standard techniques. 4-µm sections were deparaffinized, rehydrated, and incubated with blocking solution. Sections were incubated overnight at 4°C with antibodies against GFP (Life Technologies), followed by signal amplification using the TSA Fluorescein system (Perkin Elmer) or

with CD3 antibody (dilution 1:500, A0452, Dako) followed by the fluorescently-labeled secondary antibody goat anti-rabbit AlexaFluor-555 (dilution 1:200, A21428, Molecular Probes, Thermofisher). Insulitis score was evaluated by Hematoxylin-Eosin staining of formalin-fixed paraffin embedded pancreata sections. A score ranging from 0 to 3 was assigned to each identified islet by manual bright field microscope visualization (0: intact islet; 1: peri-insulitic islet; 2: <50% infiltrated islet area; 3: > 50% infiltrated islet area) (Figure S8).

Immunofluorescence analysis was performed to quantify insulin, glucagon and Cxcl10 positive volume. 5µm formalin-fixed paraffin embedded pancreata sections were subjected to double or triple immunofluorescence staining using respectively polyclonal guinea pig anti-insulin (dilution 1:500, A0564, Dako), monoclonal mouse anti-glucagon (dilution 1:300, MAB1249, R&D Systems) and polyclonal rabbit anti-murine CXCL10 (dilution 1:25, 500-P129, Peprotech); fluorescently-labeled secondary antibodies were goat anti-guinea pig Alexa-Fluor 488 (dilution 1:500, A11073, Molecular Probes, Thermofisher), goat anti-mouse 647 (dilution 1:500, A21236, Molecular Probes, Thermofisher) or goat anti-rabbit Alexa-Fluor 594 conjugated (dilution 1:500, A11037, Molecular Probes, Thermofisher). Stained sections were imaged and analyzed using Leica Sp5 confocal microscopy. Five different focal planes for each identified islet were scanned at 40X magnification. The analysis of positive insulin and CXCL10 volume (µm3) and CXCL10-insulin and CXCL10-glucagon colocalization rate (%) was quantified using Volocity 6.3 software (Perkin Elmer) by measuring the quantity of insulin and CXCL10 positive fluorescent voxels signal in five different focal planes of each scanned islet and by measuring the ratio between double positive voxels CXCL10-insulin and CXCL10-glucagon on total insulin and glucagon positive voxels for each scanned islet.

Immunofluorescence analysis to quantify insulin, glucagon and FoxP3+ cells, was performed by triple immunofluorescence staining with polyclonal guinea pig anti-insulin (dilution 1:500, A0564, Dako), monoclonal mouse anti-glucagon (dilution 1:300, MAB1249, R&D Systems) and rat monoclonal anti-murine FoxP3, FITC conjugated (dilution 1:100, 11-5773-82, eBioscience); fluorescent labeled

secondary antibodies goat anti-guinea pig Alexa Fluor 405 conjugated (dilution 1:500, Ab175678, Abcam), goat anti-mouse 594 conjugated (dilution 1:500, A11032, Molecular Probes, Thermofisher), Rabbit anti-fluorescein 488 conjugated (dilution 1:80, A11090, Molecular Probes, Thermofisher) and tertiary antibody goat anti-rabbit 488 conjugated (dilution 1:200, A11034, Molecular Probes, Thermofisher), were used. Stained sections were imaged and analyzed using Leica Sp5 confocal microscopy as described above and FoxP3+ cells were quantified through manual cell count.

QUANTIFICATION AND STATISTICAL ANALYSIS

Data are expressed as mean ± SD. Statistical significance was determined using parametric unpaired two-tailed Student's *t*-test or, for multiple comparisons, with one-way analysis of variance (ANOVA) of the means, followed by post-hoc Dunnett or Tukey test, or unparametric Mann-Whitney U test (Graph Pad Prism6). The percentage of nondiabetic mice was calculated by Kaplan–Meier survival analysis and were compared using the Log rank (Mantel-Cox) test. P values less than 0.05 ($p < 0.05$) were considered statistically significant.

DATA AND SOFTWARE AVAILABILITY

The accession number for the genomic data reported in this paper is Gene Expression Omnibus: GSE92439.

Figure

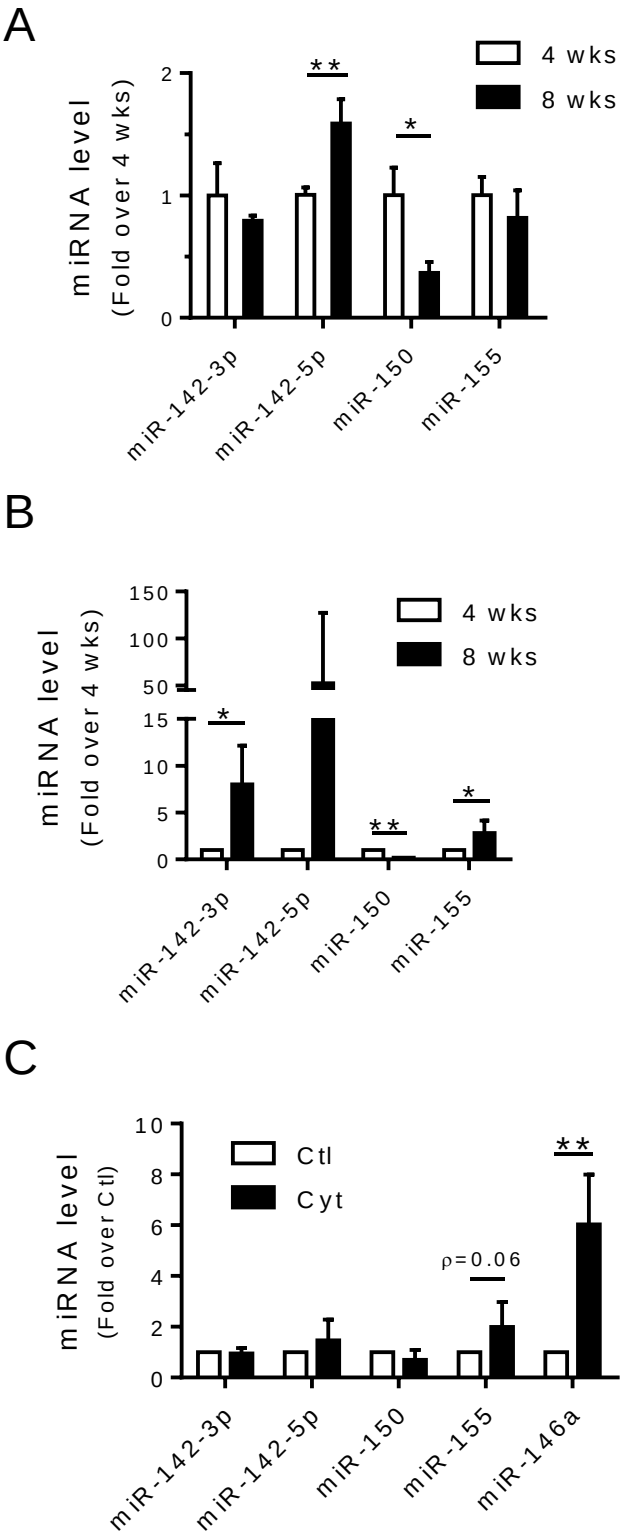

Figure 1 Guay et al.

Figure

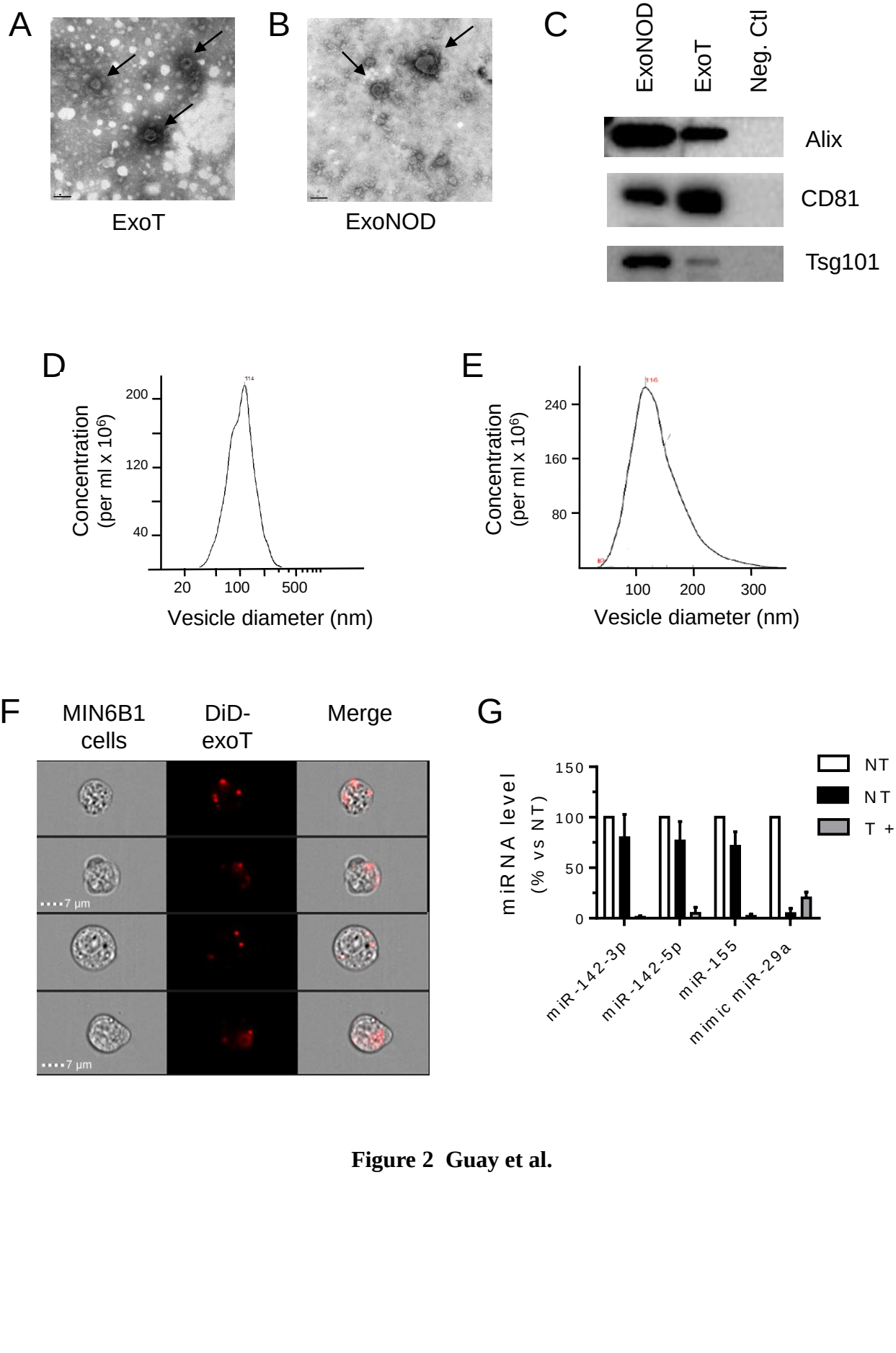

Figure 2 Guay et al.

Figure

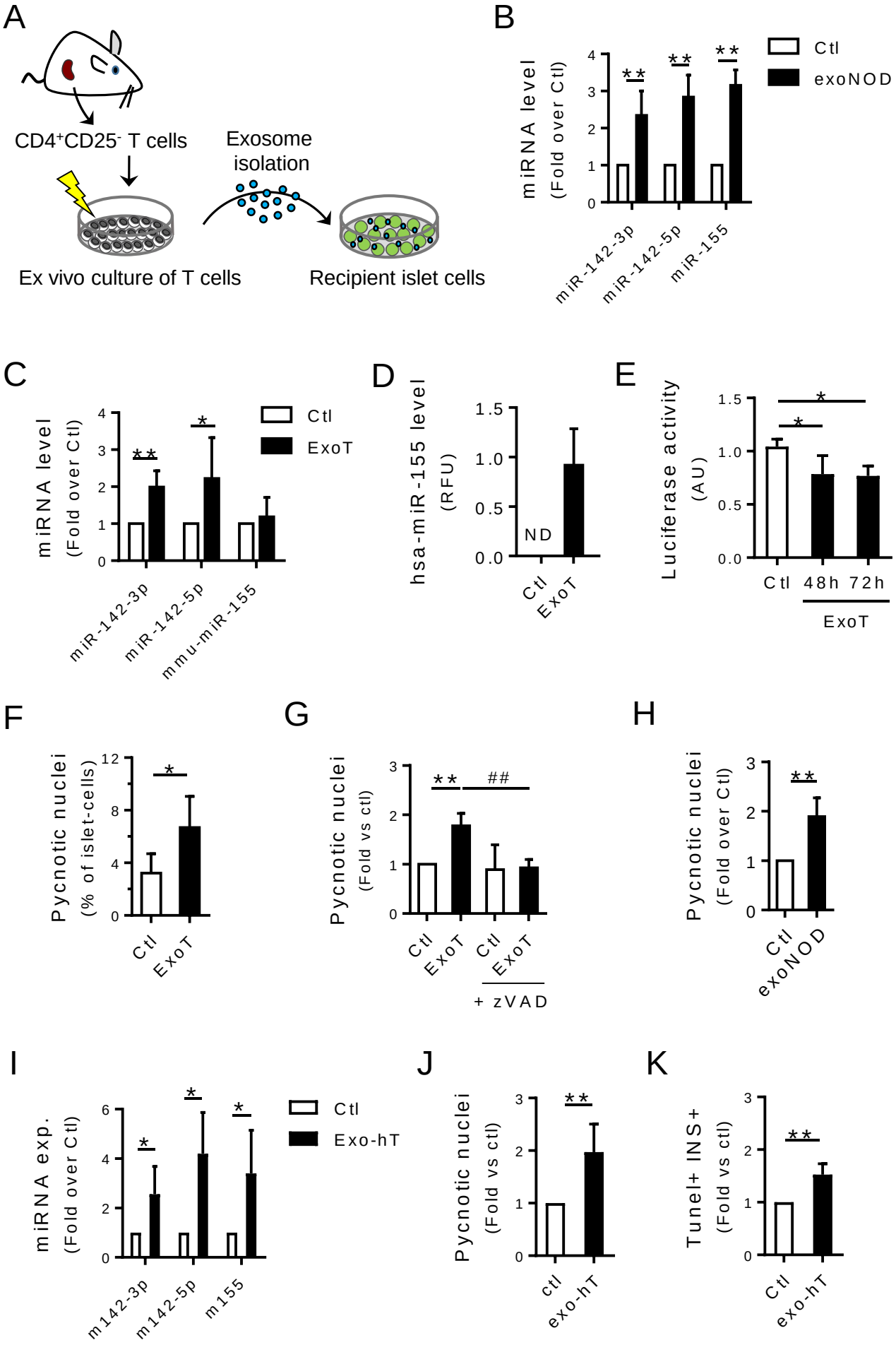

Figure 3 Guay et al.

Figure

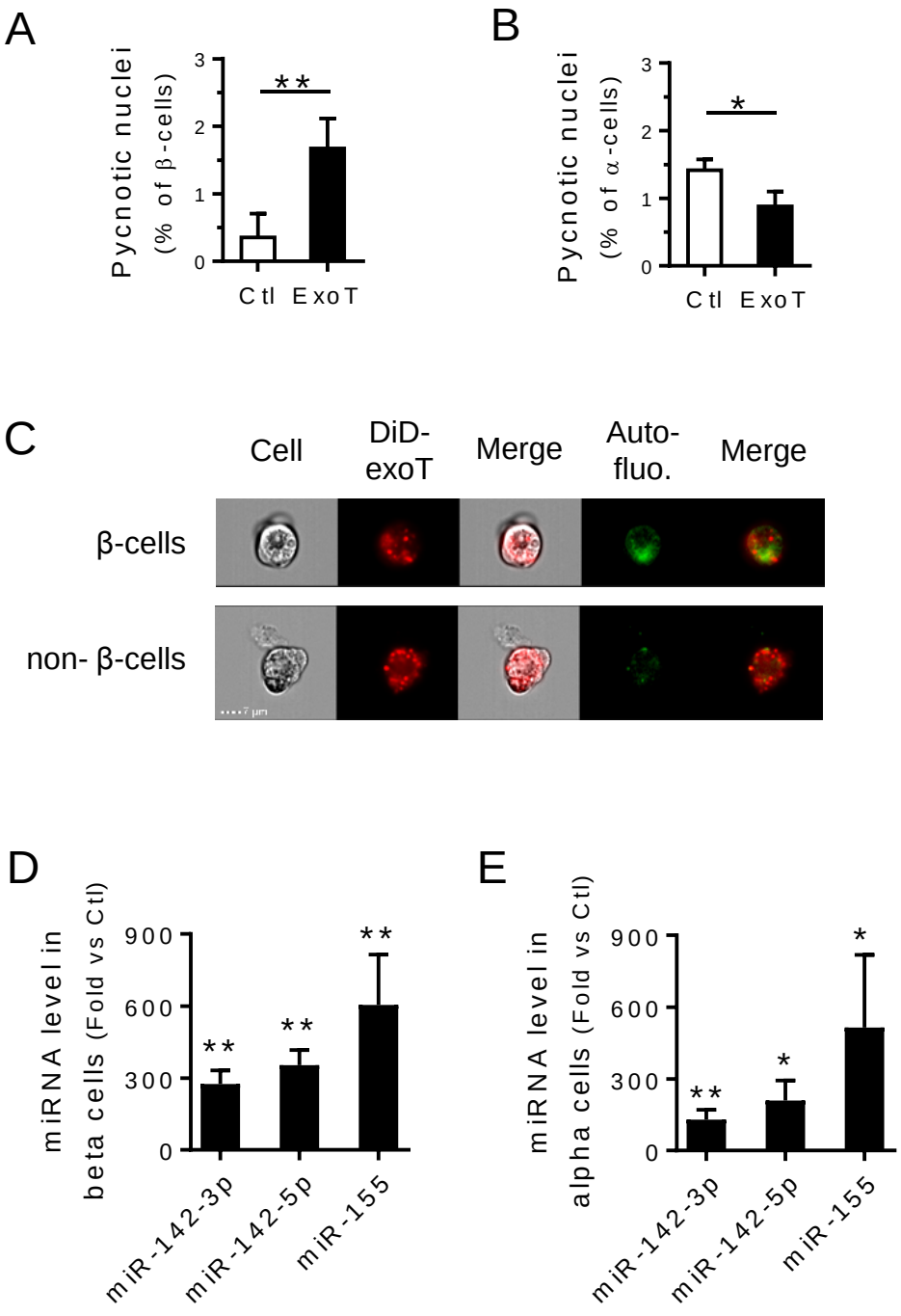

Figure 4 Guay et al.

Figure

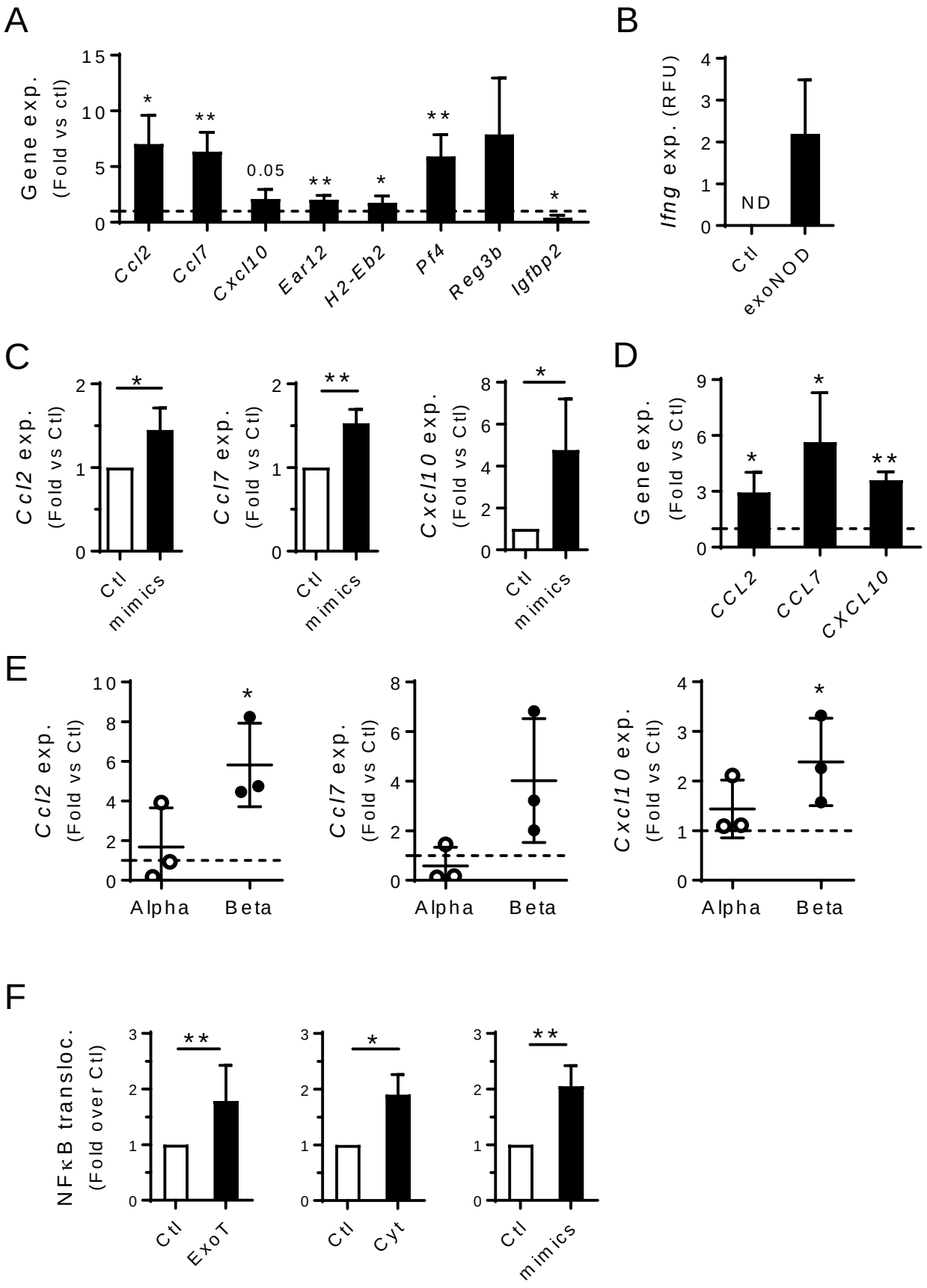

Figure 5 Guay et al.

Figure

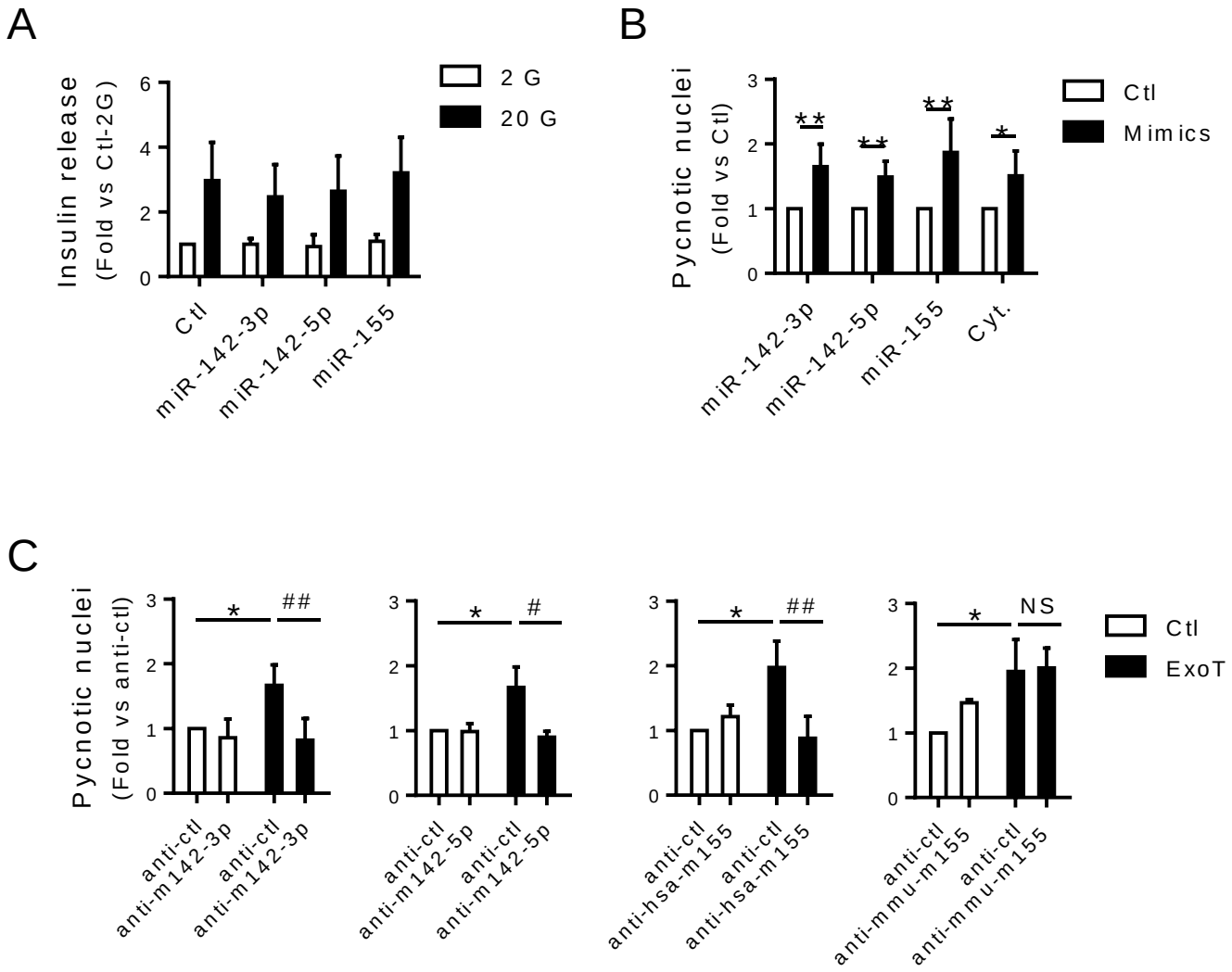

Figure 6 Guay et al.

Figure

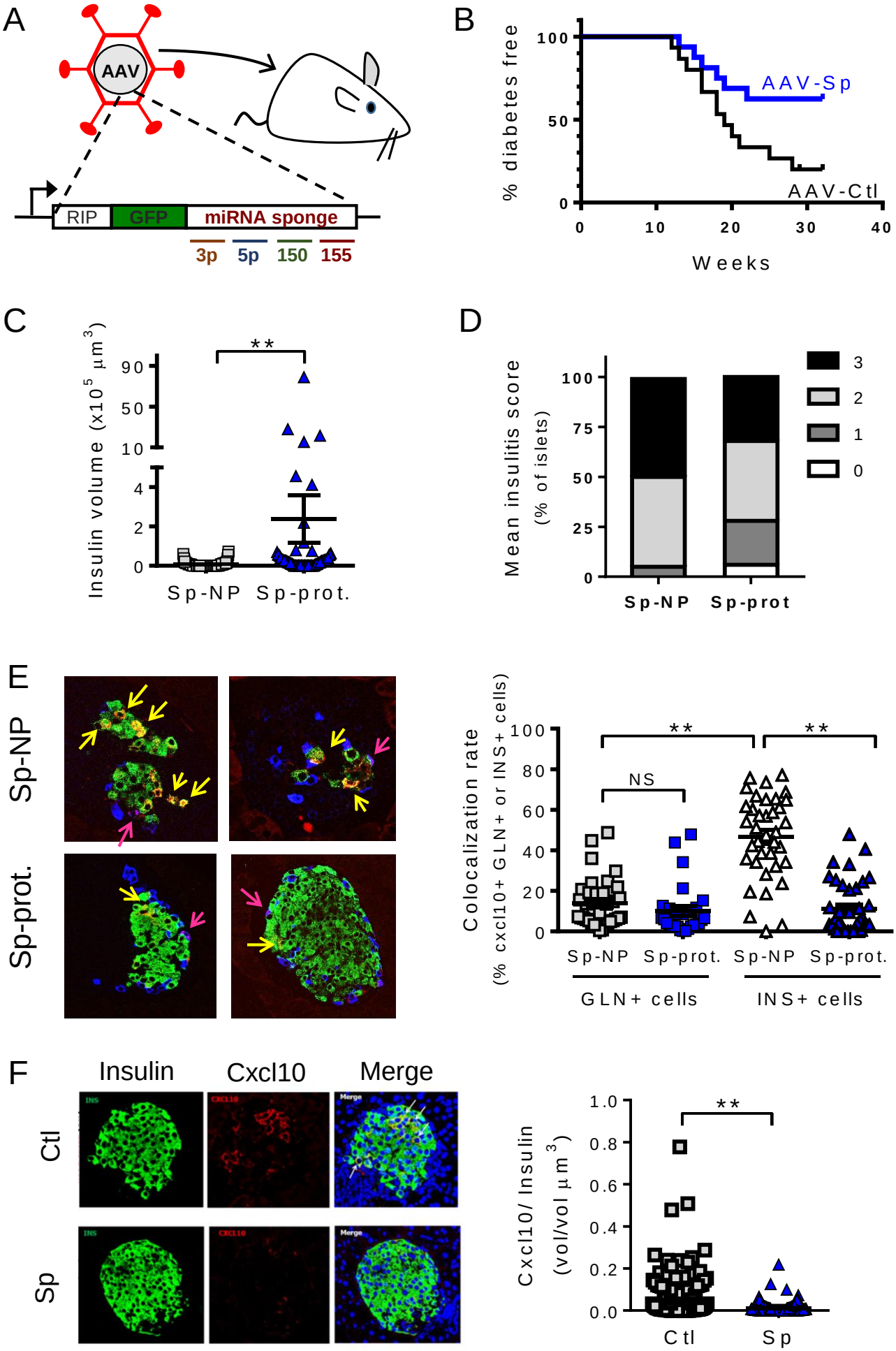

Figure 7 Guay et al.

KEY RESOURCES TABLE

REAGENT or RESOURCE	SOURCE	IDENTIFIER
Antibodies		
Alix 1:1000	Santa Cruz Biotechnology	Cat# sc-49268 RRID: AB_2268130
CD3 1:500	Dako	Cat# A0452 RRID: AB_2335677
CD4+ CD25+ Regulatory T Cell Isolation Kit, mouse	Miltenyi	Cat#130-091-041
CD81 1:1000	Santa Cruz Biotechnology	Cat# sc-166028 RRID: AB_2275895
CXCL10 1:25	Peprotech	Cat# 500-P129 RRID: AB_147769
Fluorescein 1:80	Thermofisher	Rabbit; Alexa 488; Cat# A11090 RRID: AB_221562
FoxP3, FITC conjugated 1:100	eBioscience	Cat# 11-5773-82 RRID: AB_465243
Glucagon 1:1000 (ICC)	Abcam	Cat# Ab10988 RRID: AB_297642
Glucagon 1:300 (IHC)	R&D Systems	Cat# MAB1249 RRID: AB_2107340
IgG (Guinea Pig) 1:500	Abcam	Goat; Alexa 405; Cat# Ab175678
IgG (Guinea Pig) 1:500	Thermofisher	Goat; Alexa 488; Cat# A11073 RRID: AB_142018
IgG (Guinea Pig) 1:400	Thermofisher	Goat; Alexa 555; Cat# A21435 RRID: AB_1500610
IgG (Mouse) 1:500	Thermofisher	Goat; Alexa 488; Cat# A11029 RRID: AB_138404
IgG (Mouse) 1:500	Thermofisher	Goat; Alexa 555; Cat# A21422 RRID: AB_141822
IgG (Mouse) 1:500	Thermofisher	Goat; Alexa 594; Cat# A11032 RRID: AB_141672
IgG (Mouse) 1:500	Thermofisher	Goat; Alexa 647; Cat# A21236 RRID: AB_ 2535805
IgG (Rabbit) 1:200	Thermofisher	Goat; Alexa 488; Cat# A11034 RRID: AB_ 2576217
IgG (Rabbit) 1:200	Thermofisher	Goat; Alexa 555; Cat# A21428 RRID: AB_141784
IgG (Rabbit) 1:500	Thermofisher	Goat; Alexa 594; Cat# A11037 RRID: AB_2534095

Insulin 1:100 (ICC) or 1:500 (IHC)	Dako	Cat# A0564 RRID: AB_10013624
Insulin 1:10 (human)	Dako	Cat# IR00261-2
NFκB p65 1:100	Santa Cruz Biotechnology	Cat# sc-372 RRID: AB_10013624
TSG101 1:1000	Santa Cruz Biotechnology	Cat# sc-6037 RRID: AB_2208099
Bacterial and Virus Strains		
dsAAV8-RIP-GFP-sponge	This paper	N/A
dsAAV8-RIP-GFP-control	This paper	N/A
Biological Samples		
Non-diabetic; 53 years; M; 27.2 BMI; human islets (80% purity, 90% viability) (organ donor)	CEED in Strasbourg, France	N/A
Non-diabetic; 39 years; F; 31.4 BMI; human islets (70% purity, 90% viability) (organ donor)	CEED in Strasbourg, France	N/A
Non-diabetic; 43 years; F; 34.0 BMI; human islets (90% purity, 95% viability) (organ donor)	Tebu-Bio	HP-18157-01
Non-diabetic; 50 years; F; 19.6 BMI; human islets (80% purity, 95% viability) (organ donor)	CEED in Strasbourg, France	N/A
Chemicals, Peptides, and Recombinant Proteins		
DiD (Vybrant™ Multicolor Cell-Labeling Kit)	Molecular Probes	Cat# V22889
Dynabeads T-activator CD3/CD28, human	Invitrogen	Cat# 11132D
Dynabeads T-activator CD3/CD28, mouse	Invitrogen	Cat# 11456D
Hoechst 33342	Invitrogen	Cat# H21492
IFNγ, mouse	R&D system Europe	Cat# 485-MI
IL-1β, mouse	Peprotech	Cat# 211-11B
IL-2, human	R&D system Europe	Cat# 200-02
IL-2, mouse	R&D system Europe	Cat# 212-12
IL-12, mouse	R&D system Europe	Cat# 210-12
pan caspase inhibitor Z-VAD-FMK	R&D system Europe	Cat# FMK001
TNFα	Peprotech	Cat# 315-01A
Critical Commercial Assays		
FluoroCet exosome quantification kit	System Biosciences	Cat# FCET96A-1
Deposited Data		
Raw microarray data	This paper	GSE92439
Experimental Models: Cell Lines		
Jurkat cells, J77 clone 20	O. Acuto	Rebeaud et al., 2008
MIN6B1 cell line	PA Halban	Lilla et al., 2003
Experimental Models: Organisms/Strains		
Wistar Han IGS Rat	Charles River	Cat# 2308816 RRID:RGD_2308816

JAX™ NOD/ShiLtJ Mice	Charles River	Cat# JAX:001976 RRID:IMSR_JAX:001976
NOD.CB17/Prkdc$^{scid/scid}$/Rj	Janvier	Cat# SM-NOD
B6.Cg-Mir155tm1Rsky/J	Jackson	Cat# JAX:007745 RRID:IMSR_JAX:007745
C57Bl/6N mice	Janvier	JAX:005304 RRID:IMSR_JAX:005304
Oligonucleotides		
miRCURY LNA inhibitor Control (Neg A)	Exiqon	Cat# 199004-00
hsa-miR-142-3p miRCURY LNA miRNA Inhibitor	Exiqon	Cat# 410060-00
hsa-miR-142-5p miRCURY LNA miRNA Power Inhibitor	Exiqon	Cat# 426805-00
hsa-miR-155-5p miRCURY LNA miRNA Inhibitor	Exiqon	Cat# 410078-00
mmu-miR-155-5p miRCURY LNA miRNA Inhibitor	Exiqon	Cat# 411222-00
Negative Control 4 miRCURY LNA miRNA Mimic	Exiqon	Cat# 479903-001
hsa-miR-29a miRCURY LNA miRNA Mimic	Exiqon	Cat# 472650 -001
hsa-miR-142-3p miRCURY LNA miRNA Mimic	Exiqon	Cat# 470805-001
hsa-miR-142-5p miRCURY LNA miRNA Mimic	Exiqon	Cat# 470908-001
mmu-miR-155 miRCURY LNA miRNA Mimic	Exiqon	Cat# 470919-001
hsa-miR-7-5p PCR primers	Exiqon	Cat# 205877
hsa-miR-29a-3p PCR primers	Exiqon	Cat# 204698
hsa-miR-142-3p PCR primers	Exiqon	Cat# 204291
hsa-miR-142-5p PCR primers	Exiqon	Cat# 204722
hsa-miR-146a PCR primers	Exiqon	Cat# 204688
hsa-miR-150-5p PCR primers	Exiqon	Cat# 204660
hsa-miR-155-5p PCR primers	Exiqon	Cat# 204308
mmu-miR-155-5p PCR primers	Exiqon	Cat# 205930
Recombinant DNA		
psicheck1 vector - hsa-miR-155 binding sequence in the 3'UTR	R. Renne	Skalsky et al. 2007
psicheck1 vector - ctl	Promega	Cat#: C8011
Software and Algorithms		
Volocity 6.3 software	Perkin Elmer	RRID:SCR_002668
Graph Pad Prism 6	Graph Pad software	https://www.graphpad.com/scientific-software/prism/

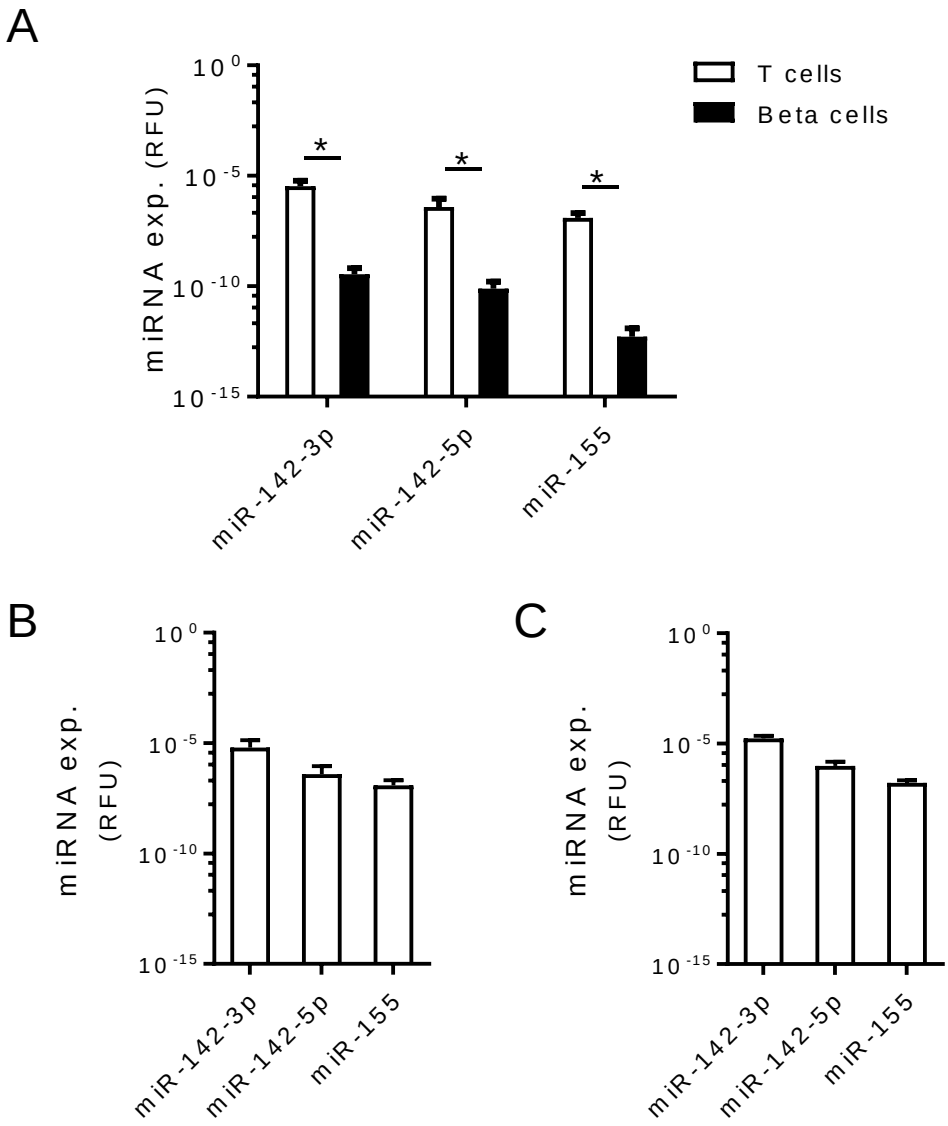

Figure S1: **miRNA levels in exosomes, T lymphocytes and pancreatic islet cells. Related to Figure 1.** miRNA levels were measured by qPCR from 200 ng of RNA, from A) NOD T lymphocytes (white bars) and FACS-sorted beta-cells (black bars), B) exoT and C) exoNOD. Results were calculated using the $2^{-\Delta C(T)}$ method and are presented as Relative Fluorescent Units (RFU) in log scale (n=3 indep. exp.). * $p<0.05$ by Student's *t*-test.

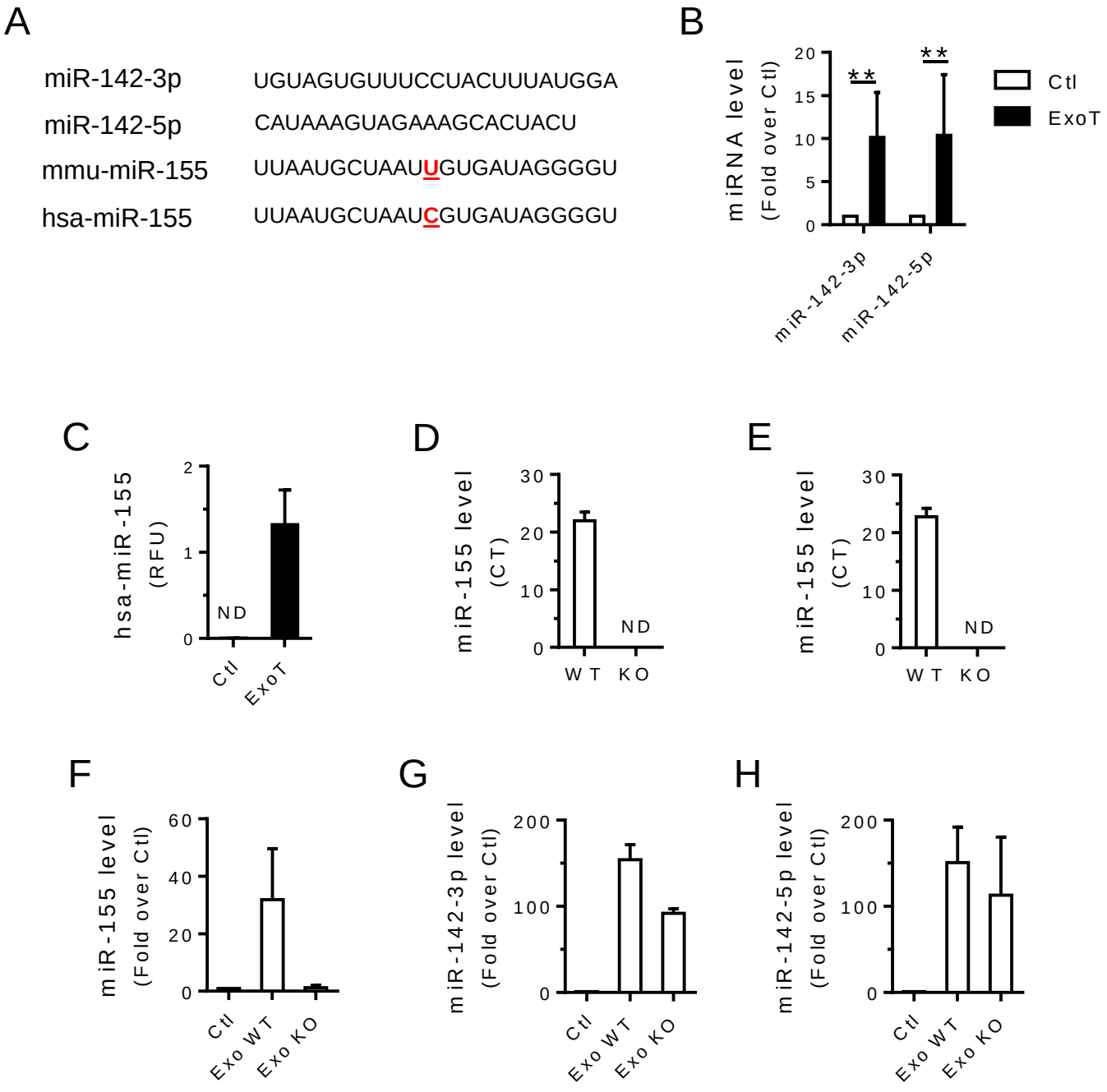

Figure S2: Transfer of exosomal miRNAs to MIN6B1 cells. Related to Figure 3. A) Mature miRNA sequences. B-C) Levels of the indicated miRNAs in MIN6B1 cells incubated for 72h with exoT (n=5-7 indep. exp.). D-H) T cells were isolated from the spleen of wild-type (WT) or KO miR-155 (KO) mice and cultured ex vivo for exosome isolation. miR-155 expression in D) T cells or E) exosomes from WT or miR-155 KO mice (n=3 indep. exp.). F-H) MIN6B1 cells were incubated with exosomes from WT or KO T cells (exoWT or ExoKO) for 72h prior to RNA extraction and measurement of miR-155 (F), miR-142-3p (G) and miR-142-5p (H) (n=3 indep. exp.). miRNA levels were measured by qPCR, normalized to miR-7 and expressed as fold changes over Ctl or as RFU (Relative Fluorescent Unit) if not detected (ND) in Ctl condition. miR-155 expression in T cells and in exosomes are presented as CT. **Significantly different from Ctl condition, $p<0.01$ by Student's *t*-test.

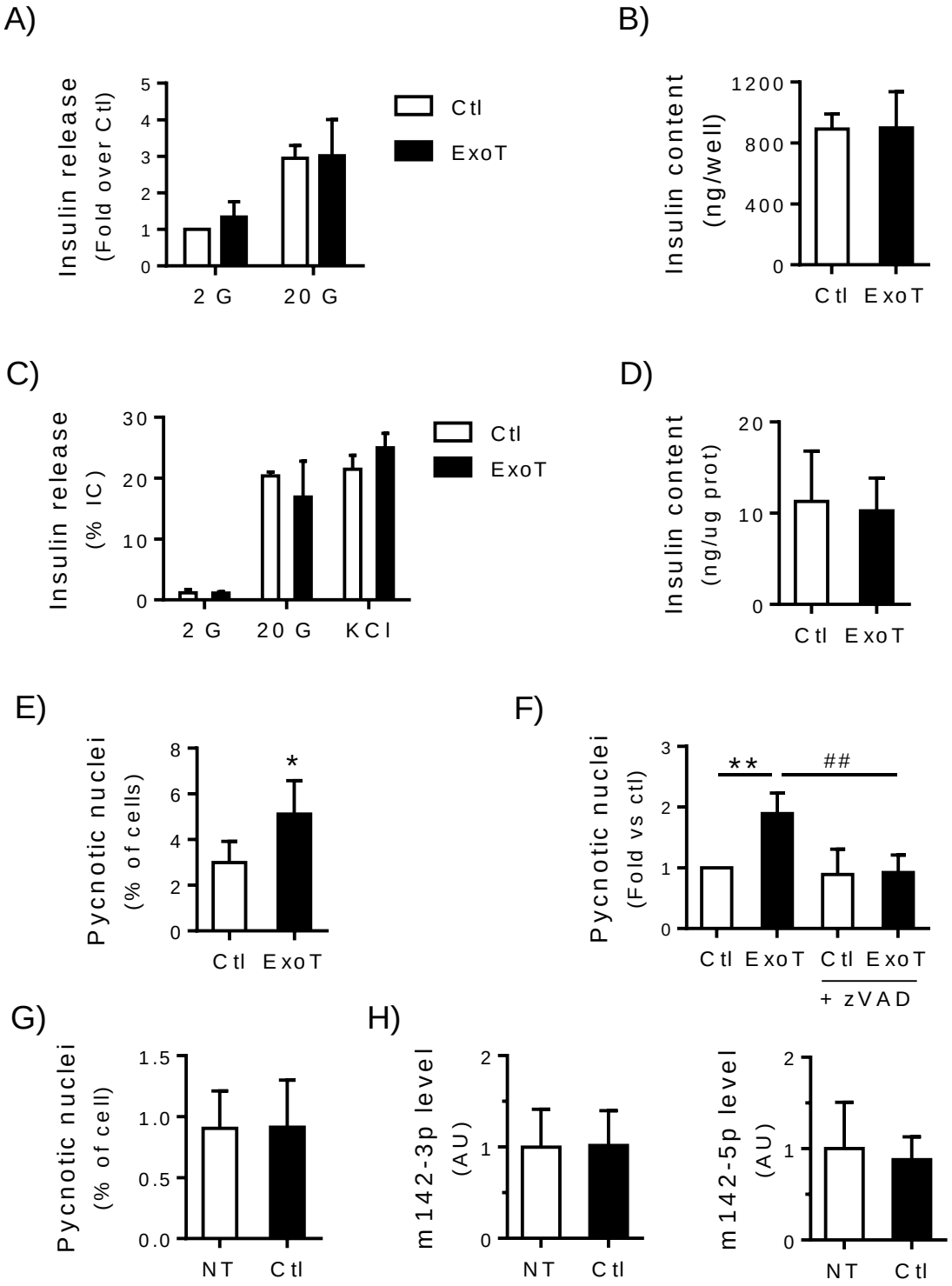

Figure S3: **Effects of exoT on beta-cell function and survival. Related to Figure 3.** Dispersed rat islet (A-B) or MIN6B1 (C-H) cells were incubated for 72h without treatment (NT), with control supernatant (Ctl) or with exosomes isolated from culture media of Jurkat cells (exoT). At the end of the incubation period, A,C) insulin release in response to 2 or 20 mM glucose (2-20G) or to 35 mM KCl, and B,D) insulin content, were measured by ELISA (n=3 indep. exp.). E-G) Apoptosis was assessed by scoring the cells displaying pycnotic nuclei upon Hoechst staining, with or without the pan-caspase inhibitor zVAD (E: n=6, F: n=4, G: n=3 indep. exp.). H) miR-142-3p and miR-142-5p levels were measured by qPCR and normalized to miR-7 (n=4). *Significantly different from Ctl condition # Significantly different from ExoT condition (without Z-VAD). *p<0.05 or **,## p<0.01 by Student's *t*-test or, for multiple comparisons, by one-way Anova, Dunnett's post-hoc test.

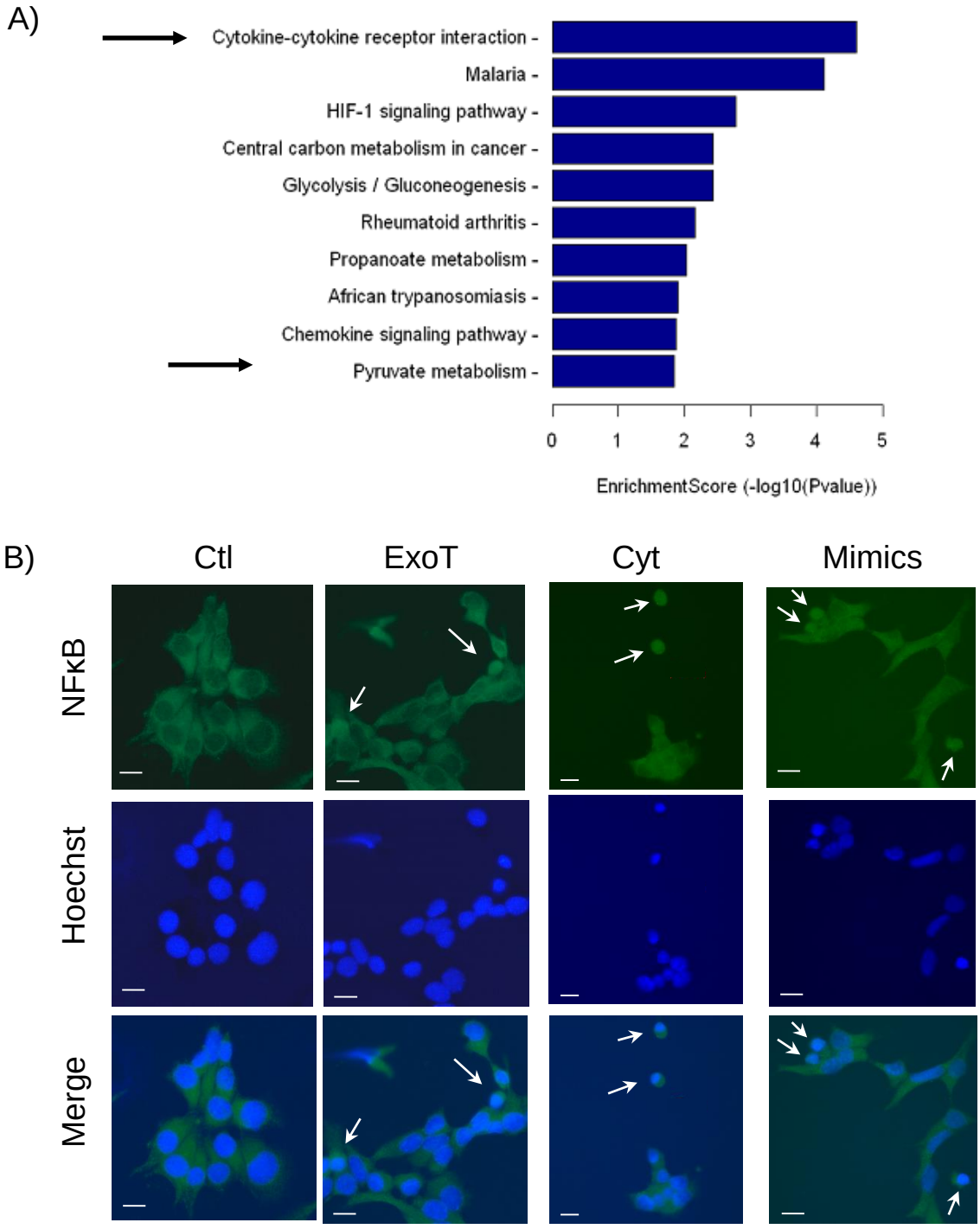

Figure S4: **Signaling pathways activated in response to exosomes. Related to Figure 5.** A) KEGG pathway enrichment analysis of genes differentially expressed in mouse islet cells incubated with exoNOD. The bars show the Enrichment score (-log10 p-value) of the indicated pathways in the array data set. Modified Fisher's exact test (EASE cutoff $p<0.05$) was used to estimate the false discovery rate (FDR) and the thresholds to select significantly enriched KEGG pathways (n=3 indep. exp.). B) Representative pictures of NFκB translocation to the nucleus. MIN6B1 cells were incubated with exoT for 72h or a mix of pro-inflammatory cytokines (cyt.: IFNγ, TNFα and IL-1β) for 24h, or were transfected with miRNA mimics leading to overexpression of miR-142-3p, miR-142-5p and miR-155 for 48h (Mimics). At the end of the incubation period, cellular localization of NFκB was determined by immunostaining. White arrows indicate positive cells with NFκB predominantly inside the nucleus. Scale bar = 10µm.

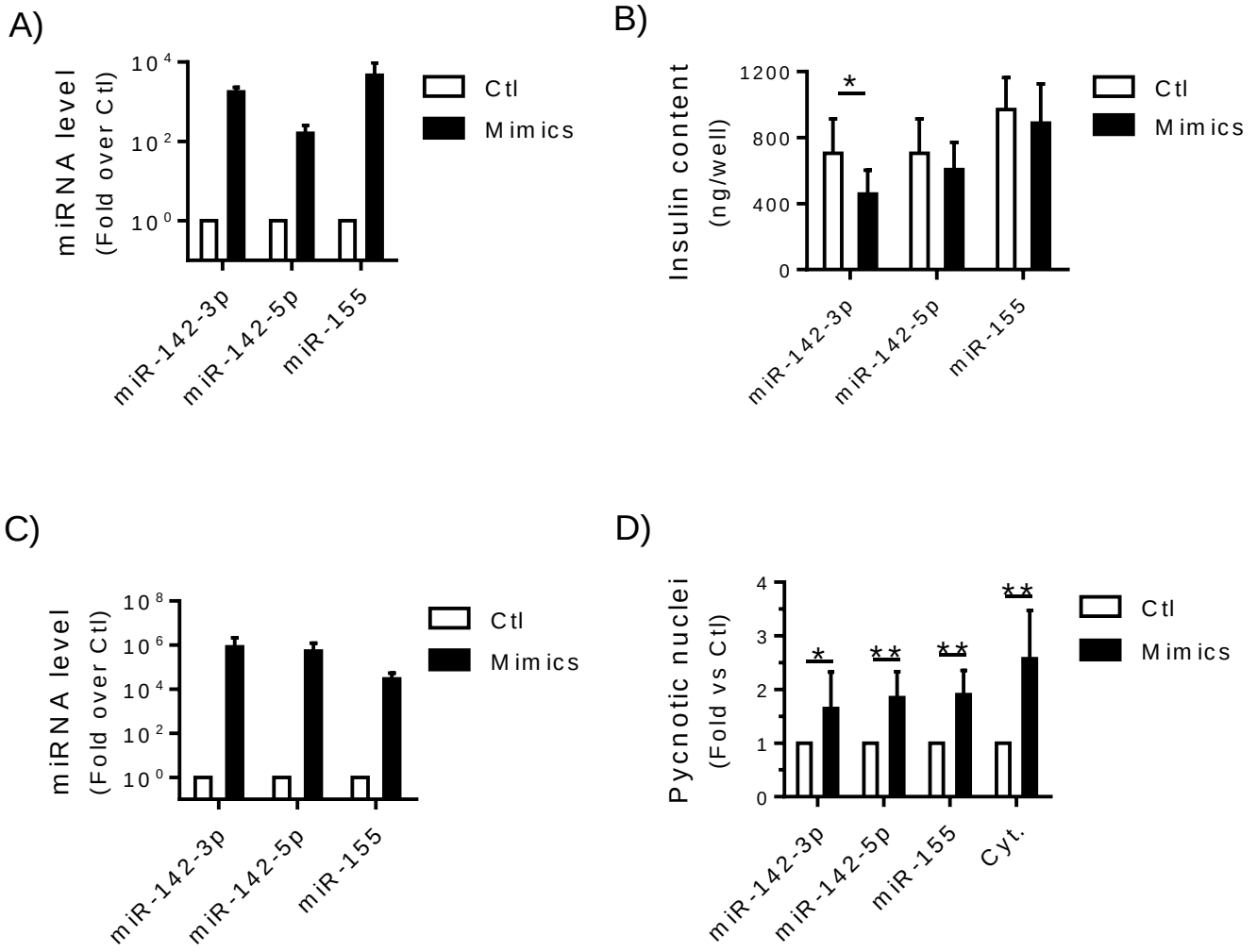

Figure S5: **Effect of miRNA overexpression on beta-cell function. Related to Figure 6.** Dispersed rat islet (A-B) or MIN6B1 (C-D) cells were transfected with the indicated miRNA mimic. Expression levels or functional assays were performed 48h post-transfection. A,C) miRNA levels were measured by qPCR, normalized to miR-7 and expressed as fold change over Ctl (n=3). B) Insulin content was measured by ELISA (n=3-4 indep.exp.). D) Apoptosis was assessed by scoring MIN6B1 cells displaying pycnotic nuclei upon Hoechst staining. Cytokine treatment (Cyt) was used as a positive control (n=4-7). *p<0.05 **p<0.01 by Student's *t*-test.

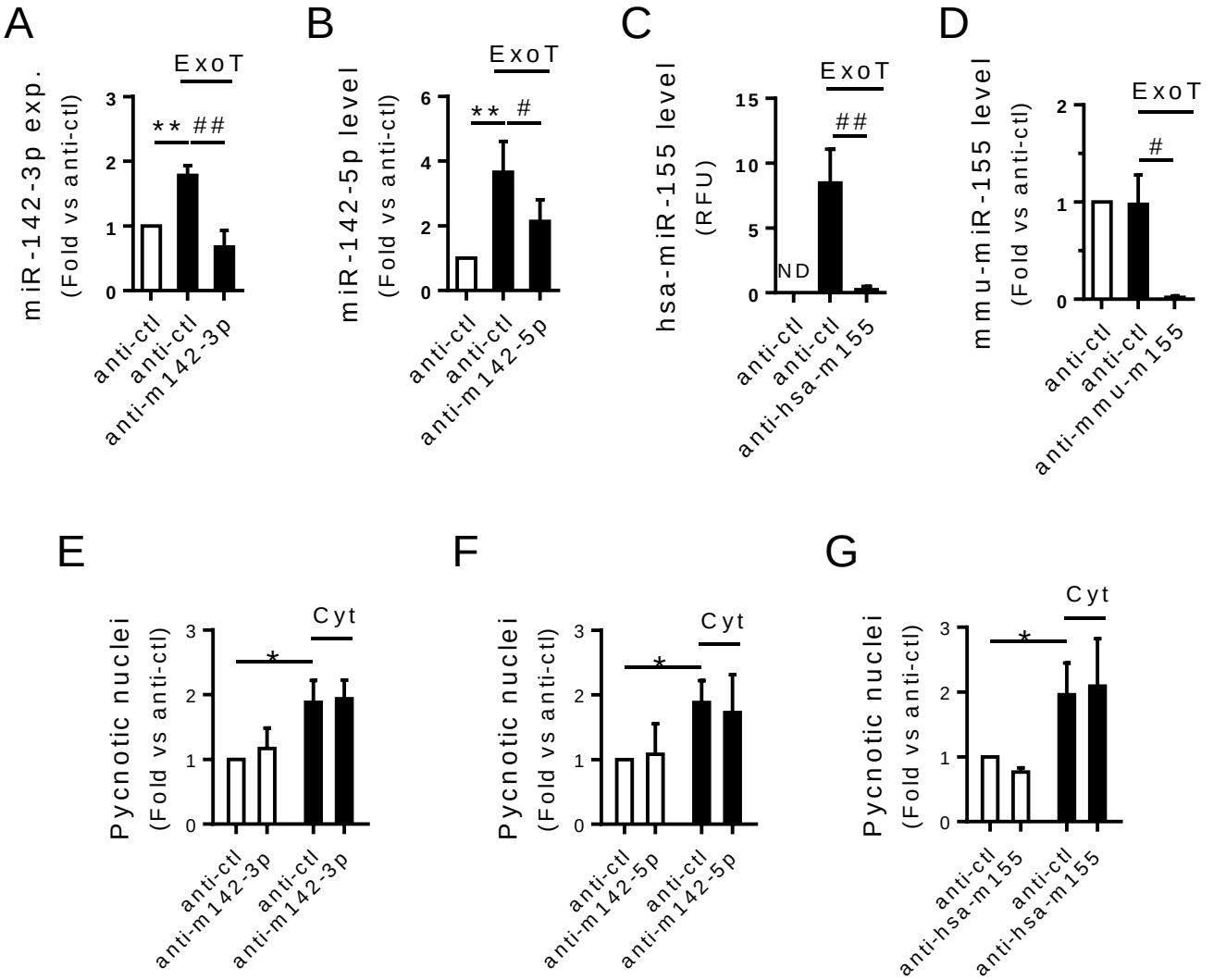

Figure S6: **Downregulation of miRNAs using anti-miRs and their effect on beta-cell survival. Related to Figure 6.** Dispersed rat islet cells were transfected with anti-miR to specifically downregulate A,E) miR-142-3p (n=4), B,F) miR-142-5p (n=4), C,G) hsa-miR-155 (n=4) or D) mmu-miR-155 (n=4 indep. exp.) and were incubated with A-D) exoT for 72h or E-G) a cytokine mix for 24h (black bars). A-D) miRNA levels in islet cells were measured by qPCR. The data are expressed as fold changes versus the anti-ctl, not treated, condition. Since hsa-miR-155 is not detected in untreated cells, results are expressed as relative fluorescence unit (RFU, derived from qPCR CT). ND= below qPCR detection limit. E-G) Apoptosis was determined by scoring the cells displaying pycnotic nuclei upon Hoechst staining. Data are expressed as fold changes versus the anti-ctl, not treated, condition. *,#$p<0.05$, **,## $p<0.01$ by one-way Anova, Dunnett's post-hoc test.

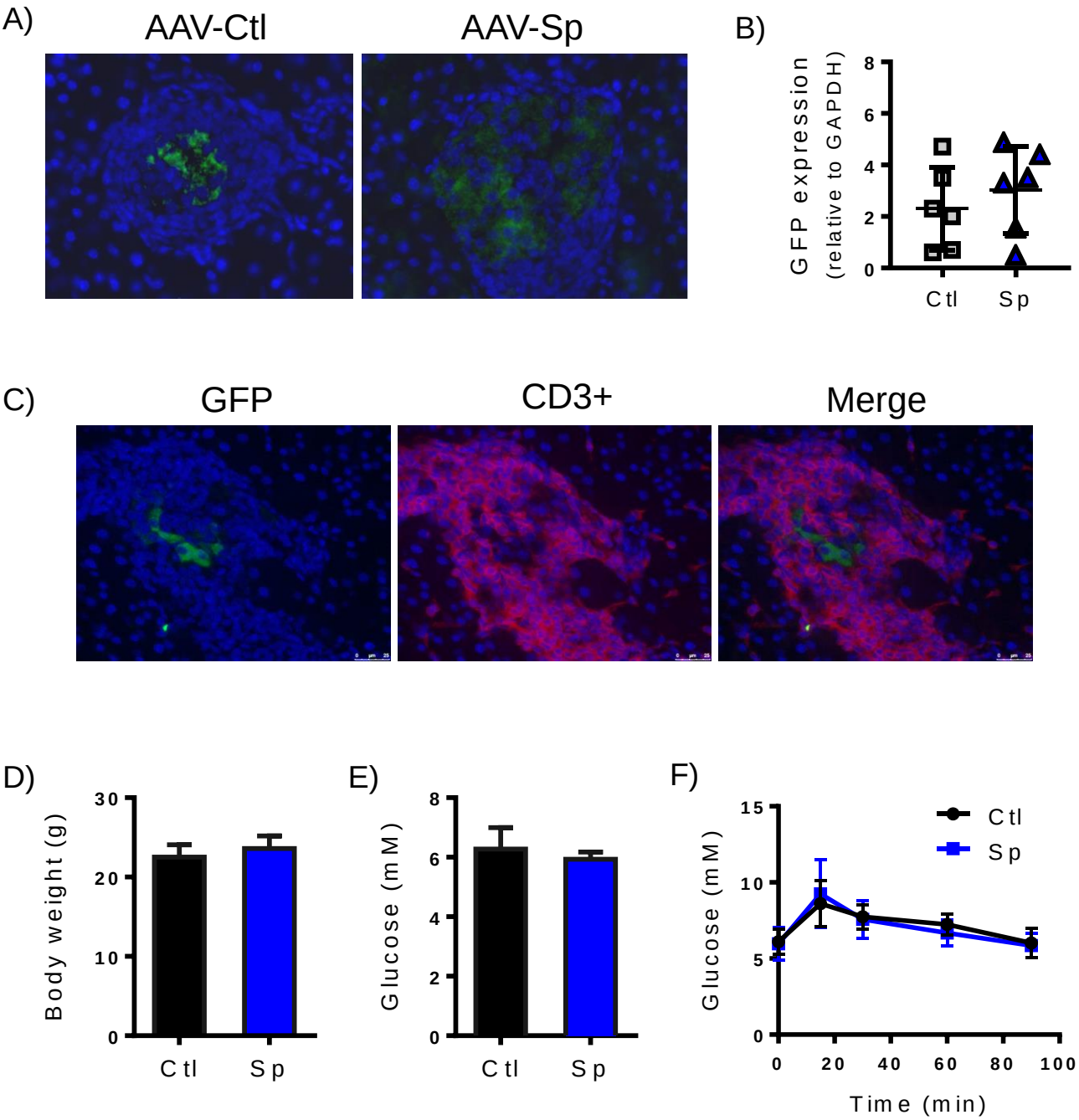

Figure S7: **Characterization of female NOD mice injected with AAV-control or AAV-sponge. Related to Figure 7.** 4 week-old female NOD mice were injected intraperitoneally with an AAV-control (Ctl) or with an AAV producing the microRNA sponge (Sp). A-C) GFP expression produced by the AAV construct was detected in NOD mice of 8 weeks of age on pancreatic sections by immunostaining (A,C), or (B) in isolated islets by qPCR (normalized to GAPDH) (n=6). C) GFP expression (Green) was not detected in immune cells marked with CD3 antibody (Red). Nuclei were stained with Dapi (Blue). D) Body weight and E) plasma glucose level were measured at 8 weeks of age (n=7). F) Intraperitoneal glucose tolerance test (1.5g/kg) was performed on 4h fasted NOD female at 10 weeks of age (n=10).

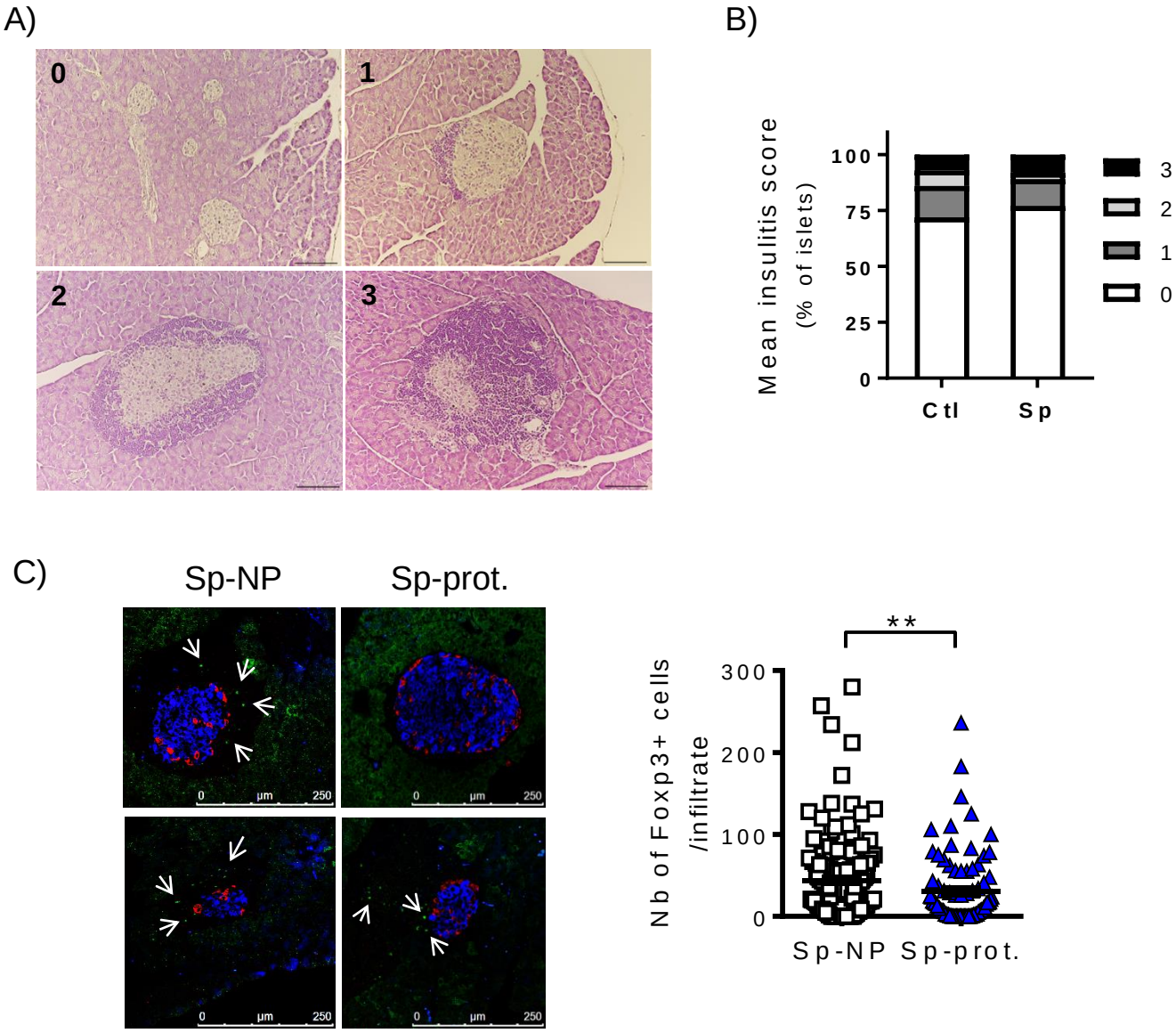

Figure S8: Infiltration and inflammation status of islets of NOD mice injected with AAV-control or AAV-sponge. Related to Figure 7.

A) Representative images of insulitis score classification analysis in NOD mice. Hematoxylin/Eosin staining on FFPE NOD mouse pancreata sections showing: Score-0: intact and not infiltrated islets, Score-1: islets with peri-insulitis, Score-2: islet with moderate insulitis with immune cells within less than 50% of islet area, and Score-3: islet with heavy insulitis with immune cells within more than 50% of islet area. Scale bar 100µm. B) Insulitis score measured in the pancreases of 8 weeks old AAV-control (Ctl) or AAV-sponge (Sp) injected mice (n=7 mice per group). C) Number of FoxP3+ T reg cells (green, arrow) per infiltrate measured in pancreases of NOD mice injected with AAV-sponge protected (Sp-Prot) or not (Sp-NP) from diabetes development, at the time of sacrifice. (insulin marked in blue and glucagon in red). ** $p < 0.01$ by Mann-Whitney U test.

Table S1: Specificity of human versus mouse miR-155 primer. Related to Figure 3.
hsa-miR-155 and mmu-miR-155 level were measured from 200ng of indicated sample.

Samples		mmu-miR-155		hsa-miR-155	
Origin	**Name**	**CT**	**RFU (2^{-ct})**	**CT**	**RFU (2^{-ct})**
Human	exoT	ND	-	28.16	3.33E-09
	Jurkats	ND	-	27.06	7.15E-09
	Islets	ND	-	26.03	1.46E-08
Rodent	Rat islets	31.20	4.06E-10	ND	-
	Mouse islets	30.50	6.60E-10	ND	-
	MIN6B1 cells	34.25	4.91E-11	ND	-

ND: under the detection limit of the qPCR (CT>37)

Table S2: Effect of exoNOD on islet cell gene expression. Related to Figure 5.

Dispersed mouse islet cells were incubated without (Ctl) or with exoNOD for 72h. Analysis of mRNA expression was then performed by microarray (n=3). Genes displaying a fold change > 2 and a nominal p-value < 0.05 are presented in this Table.

Annotations			Regulation				Raw Intensity		Normalized Intensity	
Gene Symbol	Description	Genbank Accession No	Fold Change	P-value	FDR	Regulation	group-Exo	group-Ctl	group-Exo	group-Ctl
Upregulated										
Ear12	Eosinophil-associated, ribonuclease A family, member 12	NM_001012766	15.24	0.0118801	0.353	up	148.13	5.56	6.54	2.61
Pf4	Platelet factor 4	NM_019932	7.05	0.015727	0.354	up	574.64	69.88	8.94	6.13
Zfy1	Zinc finger protein 1, Y linked	NM_009570	6.52	0.0203802	0.359	up	49.91	5.20	5.19	2.49
Ccl24	Chemokine (C-C motif) ligand 24	NM_019577	6.22	0.0215034	0.360	up	137.29	22.19	6.97	4.33
Reg3b	Regenerating islet-derived 3 beta	NM_011036	6.10	0.0259424	0.367	up	64.06	7.50	5.51	2.91
Ear1	Eosinophil-associated, ribonuclease A family, member 1	NM_007894	5.71	0.0304683	0.376	up	52.82	5.78	5.12	2.61
Ear2	Eosinophil-associated, ribonuclease A family, member 2	NM_007895	5.05	0.0307279	0.377	up	278.58	37.41	7.69	5.35
Pdcd1lg2	Programmed cell death 1 ligand 2	NM_021396	4.47	0.012026	0.353	up	219.06	46.58	7.68	5.52
Grem1	Gremlin 1	NM_011824	4.43	0.0051617	0.324	up	38.97	7.65	5.10	2.96
Ccl2	Chemokine (C-C motif) ligand 2	NM_011333	4.25	0.0479823	0.400	up	2696.45	740.89	11.32	9.24
Mrc1	Mannose receptor, C type 1	NM_008625	3.89	0.0042547	0.315	up	66.66	14.13	5.90	3.94
Ccl7	Chemokine (C-C motif) ligand 7	NM_013654	3.85	0.0279532	0.372	up	498.58	133.18	8.89	6.94
Pdpn	Podoplanin	NM_010329	3.83	0.0183558	0.354	up	907.44	244.77	9.79	7.85
Serpina3g	Serine (or cysteine) peptidase inhibitor, clade A, member 3G	NM_009251	3.59	0.0196062	0.357	up	1377.21	367.88	10.34	8.50
Tnnt2	Troponin T2, cardiac	NM_011619	3.49	0.0303066	0.376	up	29.04	7.55	4.62	2.82
Ifng	Interferon gamma	NM_008337	3.13	0.0065303	0.327	up	30.62	7.38	4.71	3.06
Klra15	Killer cell lectin-like receptor, subfamily A, member 15	NM_013793	3.11	0.0021235	0.289	up	17.93	5.00	3.98	2.34
F10	Coagulation factor X	NM_007972	3.09	0.0458147	0.396	up	215.59	69.24	7.65	6.02
Apol7c	Apolipoprotein L 7c	NM_175391	3.03	0.0032293	0.299	up	63.07	17.13	5.84	4.24
Dlx5	Distal-less homeobox 5	NM_010056	3.02	0.0121578	0.353	up	103.25	27.59	6.51	4.92
Ereg	Epiregulin	NM_007950	3.00	0.0074262	0.337	up	78.52	21.38	6.13	4.54
Timp1	Tissue inhibitor of metalloproteinase 1	NM_001044384	2.94	0.0171777	0.354	up	4303.92	1401.02	11.99	10.44
Rnase10	Ribonuclease, RNase A family, 10	NM_029145	2.91	0.0021479	0.289	up	378.02	114.24	8.47	6.93
Cck	Cholecystokinin	NM_001284508	2.80	0.005592	0.325	up	529.91	170.79	8.97	7.48
Gfra2	Glial cell line derived neurotrophic factor family receptor alpha 2	NM_008115	2.80	0.011636	0.353	up	79.60	22.38	6.12	4.63
Ms4a1	Membrane-spanning 4-domains, subfamily A, member 1	NM_007641	2.78	0.0260844	0.367	up	35.31	9.77	4.91	3.44
Kank4	KN motif and ankyrin repeat domains 4	NM_172872	2.72	0.0055869	0.325	up	35.87	10.63	5.00	3.56
Cst7	Cystatin F (leukocystatin)	NM_009977	2.67	0.0214243	0.360	up	45.48	14.59	5.36	3.94
Speer4c	Spermatogenesis associated glutamate (E)-rich protein 4c	NM_001281511	2.67	0.0241672	0.364	up	116.55	35.72	6.70	5.28
Tspan10	Tetraspanin 10	NM_145363	2.65	0.0378119	0.387	up	18.45	5.35	3.89	2.49
Defb45	Defensin beta 45	NM_001037752	2.58	0.0147662	0.354	up	112.79	35.88	6.66	5.29
Olfr1410	Olfactory receptor 1410	NM_146491	2.55	0.0099897	0.349	up	672.83	236.37	9.30	7.95
Egr2	Early growth response 2	NM_010118	2.54	0.0227117	0.361	up	270.40	98.23	8.00	6.65
H2-Eb2	Histocompatibility 2, class II antigen E beta2	NM_001033978	2.54	0.0097198	0.348	up	130.00	44.23	6.91	5.57
Ccbe1	Collagen and calcium binding EGF domains 1	NM_178793	2.53	0.0104507	0.349	up	111.91	37.54	6.68	5.34
Dbh	Dopamine beta hydroxylase	NM_138942	2.48	0.0096035	0.348	up	37.53	11.61	5.02	3.71
Olfr1198	Olfactory receptor 1198	NM_207567	2.48	0.0062325	0.325	up	78.25	25.71	6.13	4.82
Chil3	Chitinase-like 3	NM_009892	2.47	0.0006986	0.226	up	129.32	44.95	6.92	5.61
Cd300a	CD300A antigen	NM_170758	2.46	0.0166578	0.354	up	1338.06	495.83	10.30	8.99
Zfp217	Zinc finger protein 217	NM_001033299	2.46	0.0143316	0.354	up	59.37	19.35	5.72	4.42
Sox3	Sex determining region Y(SRY)-box 3	NM_009237	2.42	0.0005734	0.224	up	14.27	5.00	3.62	2.34
Tpsb2	Tryptase beta 2	NM_010781	2.38	0.0010457	0.248	up	670.40	260.85	9.34	8.08
Golga7b	Golgi autoantigen, golgin subfamily a, 7B	NM_001141983	2.37	0.049228	0.400	up	1490.35	559.20	10.40	9.16
Ldhc	Lactate dehydrogenase C	NM_013580	2.36	0.0004425	0.224	up	23.24	7.81	4.38	3.14
Chat	Choline acetyltransferase	NM_009891	2.36	0.0349162	0.382	up	4214.92	1675.74	11.95	10.71
Gfap	Glial fibrillary acidic protein	NM_001131020	2.34	0.0180347	0.354	up	33.89	11.52	4.90	3.67
Rarres2	Retinoic acid receptor responder (tazarotene induced) 2	NM_027852	2.33	0.0143987	0.354	up	1883.52	773.19	10.82	9.60
Ptgir	Prostaglandin I receptor (IP)	NM_008967	2.31	0.005126	0.324	up	102.30	36.92	6.54	5.33
Nwd2	NACHT and WD repeat domain containing 2	NM_177006	2.31	0.0075801	0.340	up	41.38	14.07	5.19	3.98
Nhlh1	Nescient helix loop helix 1 (Nhlh1)	NM_010916	2.31	0.0158851	0.354	up	1491.11	595.49	10.46	9.26
Olfr1414	Olfactory receptor 1414	NM_147039	2.30	0.0387261	0.388	up	20.32	7.49	4.15	2.95
Klra4	Killer cell lectin-like receptor, subfamily A member 4	NM_010649	2.30	0.003491	0.307	up	24.60	8.57	4.46	3.26

Mrgprb3	MAS-related GPR, member B3	NM_207537	2.29	0.0119451	0.353	up	58.11	21.14	5.72	4.53
Mrc2	Mannose receptor, C type 2	NM_008626	2.28	0.0353655	0.382	up	24.12	8.69	4.42	3.23
Map3k13	Mitogen-activated protein kinase kinase kinase 13	NM_172821	2.27	0.0001938	0.188	up	33.93	12.02	4.94	3.76
Adamts14	A disintegrin-like and metallopeptidase (reprolysin type) with thrombospondin type 1 motif 14	NM_001081127	2.25	0.0026975	0.296	up	124.60	46.86	6.84	5.68
Lrp2	Low density lipoprotein receptor-related protein 2	NM_001081088	2.23	0.0019692	0.289	up	21.45	7.44	4.23	3.08
March11	Membrane-associated ring finger (C3HC4) 11	NM_177597	2.22	0.0254135	0.366	up	34.73	12.75	4.95	3.80
Ltb	Lymphotoxin B	NM_008518	2.18	0.0094444	0.348	up	36.10	13.58	5.03	3.90
Skint4	Selection and upkeep of intraepithelial T cells 4	NM_178786	2.17	0.042209	0.391	up	46.43	17.87	5.37	4.25
Arhgef15	Rho guanine nucleotide exchange factor (GEF) 15	NM_177566	2.14	0.0200645	0.357	up	3285.24	1441.61	11.62	10.52
Sp6	Trans-acting transcription factor 6 (Sp6)	NM_031183	2.14	0.0210853	0.360	up	464.39	190.00	8.75	7.65
Mbd3l1	Methyl-CpG binding domain protein 3-like 1	NM_028557	2.14	0.0289503	0.374	up	20.65	7.57	4.15	3.06
Olfr432	Olfactory receptor 432	NM_146716	2.14	0.0324781	0.380	up	26.12	9.64	4.52	3.42
Dcaf12l2	DDB1 and CUL4 associated factor 12-like 2	NM_175539	2.12	0.0203415	0.359	up	3304.48	1452.86	11.61	10.52
Tnfrsf9	Tumor necrosis factor receptor superfamily, member 9	NM_011612	2.12	0.024192	0.364	up	4056.77	1800.95	11.92	10.83
Vax2	Ventral anterior homeobox 2	NM_011912	2.12	0.0161331	0.354	up	2366.74	1047.97	11.14	10.05
Fnbp1	Formin binding protein 1	NM_001177648	2.11	0.0243936	0.365	up	4182.22	1862.79	11.96	10.88
Clec1b	C-type lectin domain family 1, member b	NM_019985	2.10	0.0132953	0.353	up	20.93	8.03	4.23	3.15
Ldha	Lactate dehydrogenase A	NM_001136069	2.10	0.0023469	0.289	up	1032.44	470.94	9.99	8.92
Sema6d	Sema domain, transmembrane domain (TM), and cytoplasmic domain, (semaphorin) 6D	NM_001291000	2.08	0.0206178	0.359	up	2311.89	1054.77	11.11	10.06
Amelx	Amelogenin, X-linked	NM_009666	2.07	0.0057547	0.325	up	14.41	5.76	3.66	2.61
Hs2st1	Heparan sulfate 2-O-sulfotransferase 1	NM_011828	2.06	0.0224912	0.361	up	1906.89	864.05	10.82	9.78
Scn8a	Sodium channel, voltage-gated, type VIII, alpha	NM_001077499	2.05	0.0146585	0.354	up	4889.26	2268.17	12.20	11.16
Gxylt2	Glucoside xylosyltransferase 2	NM_198612	2.04	0.0214981	0.360	up	5684.29	2613.52	12.40	11.37
Pdgfra	Platelet derived growth factor receptor, alpha polypeptide	NM_011058	2.04	0.0166107	0.354	up	79.67	33.54	6.19	5.16
Slc1a4	Solute carrier family 1 (glutamate/neutral amino acid transporter), member 4	NM_018861	2.04	0.0189431	0.355	up	4149.50	1937.76	11.96	10.94
Cdh11	Cadherin 11	NM_009866	2.04	0.0011886	0.249	up	474.55	214.76	8.84	7.81
Golt1a	Golgi transport 1 homolog A (S. cerevisiae)	NM_026680	2.03	0.0249666	0.365	up	2023.84	927.02	10.90	9.88
Has2	Hyaluronan synthase 2	NM_008216	2.02	3.38E-05	0.098	up	279.53	123.89	8.06	7.04
Tmprss3	Transmembrane protease, serine 3	NM_001163776	2.02	0.018425	0.354	up	4360.92	2052.55	12.04	11.02
Ifit2	Interferon-induced protein with tetratricopeptide repeats 2	NM_008332	2.02	0.0392298	0.388	up	431.74	195.02	8.66	7.64
Pot1a	Protection of telomeres 1A	NM_133931	2.02	0.0154162	0.354	up	3916.90	1837.76	11.88	10.87
Bpifc	BPI fold containing family C	NM_177772	2.02	0.0245966	0.365	up	10564.79	4911.51	13.29	12.28
Hk2	Hexokinase 2	NM_013820	2.02	0.0100239	0.349	up	841.43	392.85	9.67	8.66
Kcna4	Potassium voltage-gated channel, shaker-related subfamily, member 4	NM_021275	2.01	0.0199576	0.357	up	7096.00	3329.32	12.72	11.71
Xdh	Xanthine dehydrogenase	NM_011723	2.01	0.0020746	0.289	up	186.68	81.80	7.46	6.45
Szrd1	SUZ RNA binding domain containing 1	NM_001025608	2.00	0.0228968	0.361	up	2334.59	1100.89	11.13	10.12
Tfec	Transcription factor EC	NM_031198	2.00	0.0201551	0.358	up	75.99	31.75	6.10	5.10
Vcam1	Vascular cell adhesion molecule 1	NM_011693	2.00	0.0002573	0.205	up	252.58	112.12	7.91	6.90
Downregulated										
Igfbp2	Insulin-like growth factor binding protein 2	NM_008342	6.70	0.0094897	0.348	down	25.47	146.91	4.38	7.13
Lrp4	Low density lipoprotein receptor-related protein 4	NM_172668	3.43	0.0068546	0.330	down	16.46	46.34	3.85	5.63
Ogn	Osteoglycin	NM_008760	3.35	0.0038083	0.308	down	7.20	19.09	2.64	4.39
Olfr558	Olfactory receptor 558	NM_147093	2.84	0.0418393	0.391	down	29.47	66.86	4.64	6.15
Lama1	Laminin alpha 1	NM_008480	2.57	0.0066104	0.327	down	39.68	85.16	5.15	6.51
Slamf9	SLAM family member 9	NM_029612	2.55	0.0068058	0.330	down	106.74	247.48	6.62	7.97
Cx3cr1	Chemokine (C-X3-C motif) receptor 1	NM_009987	2.40	0.0181431	0.354	down	55.93	120.05	5.66	6.92
Klrb1b	Killer cell lectin-like receptor subfamily B member 1B	NM_030599	2.34	0.030993	0.378	down	32.65	66.51	4.85	6.08
Cd93	CD93 antigen	NM_010740	2.33	0.0131063	0.353	down	92.76	194.21	6.42	7.64
Psd3	Pleckstrin and Sec7 domain containing 3	NM_177698	2.31	0.0036671	0.307	down	23.83	44.82	4.40	5.61
Gdf6	Growth differentiation factor 6	NM_013526	2.25	0.0018827	0.284	down	29.42	54.61	4.71	5.88
Igfbp2	Insulin-like growth factor binding protein 2	NM_008342	2.24	0.0286796	0.374	down	59.80	120.28	5.75	6.91
Apoe	Apolipoprotein E	NM_009696	2.22	0.0008202	0.244	down	1732.95	3733.75	10.73	11.88
Wisp2	WNT1 inducible signaling pathway protein 2	NM_016873	2.21	0.0311692	0.378	down	234.89	464.16	7.75	8.90
Ctla2b	Cytotoxic T lymphocyte-associated protein 2 beta	NM_007797	2.06	0.0404583	0.389	down	260.17	496.51	7.92	8.96
Lactbl1	Lactamase beta-like 1	NM_001243262	2.06	0.0427477	0.391	down	9.46	14.35	2.95	3.99
Hpgd	Hydroxyprostaglandin dehydrogenase 15 (NAD)	NM_008278	2.05	0.0299584	0.375	down	10.42	16.33	3.15	4.19
Srpx	Sushi-repeat-containing protein	NM_016911	2.05	0.0018271	0.283	down	55.64	97.49	5.66	6.70
Pappa2	Pappalysin 2	NM_001085376	2.04	0.0198674	0.357	down	43.14	72.29	5.25	6.28

Cobl	Cordon-bleu WH2 repeat	NM_172496	2.02	0.0168186	0.354	down	9.90	15.74	3.10	4.12
Sparcl1	SPARC-like 1	NM_010097	2.02	0.0128579	0.353	down	176.27	332.24	7.38	8.40
Fbln5	Fibulin 5	NM_011812	2.01	0.0123647	0.353	down	101.10	178.77	6.54	7.54

Table S3: Predicted target genes common to miR-142-3p, miR-142-5 and/or miR-155. Related to Figure 5

(From TargetScan, version 7.2 March 2018)

(Genes highlighted in Green are linked to cytokine and/or NFκB signaling)

Common target genes				
all 3 miRNAs	**miR-142-3p/5p**	**miR-142-3p/miR-155**	**miR-142-5p/miR-155**	
Brwd3	Ap3m1	Acbd3	Acot12	Pura
Hhip	Arhgap35	Acvr2a	Ankfn1	Qk
Lrp1b	Arrdc3	Ago2	Arid2	Rasef
Strn3	Atg16l1	Apc	Brd1	Rcn2
Zbtb20	Brwd3	Arntl	Brwd3	Reps2
	Btbd7	Atxn1l	Camta1	Rhoq
	Cask	Bach1	Cdh12	Rnf146
	Ccnt2	Bnc2	Cdon	Rps6ka3
	Cisd2	Brwd3	Csf1r	Rps6ka5
	Clcn5	Ehf	Cyp7b1	S1pr1
	Clock	Hhip	Dhx40	Sass6
	Cpeb2	Lcor	Elavl2	Selt
	Crk	Lrp1b	Fam168a	Smad2
	Fbxo3	Mob4	Fam84a	Socs1
	Fbxo45	Nfib	Fam91a1	Sort1
	Fmn1	Picalm	Fgf12	Ssh2
	Hhip	Ppig	Fgf13	Strn3
	Ipmk	Rbm47	Fgf16	Tcf4
	Ipo7	Rheb	Gsk3b	Tle4
	Itga8	Rictor	H3f3a	Tnik
	Jmjd1c	Rreb1	Hhip	Trp53inp1
	Lrp1b	Slc38a4	Hivep2	Tspan14
	Nr3c1	Smug1	Il21	Uba3
	Nsd1	Socs6	Irf2bp2	Usp9x
	Nucks1	Sox11	Jarid2	Ywhae
	Otp	Spred1	Kcna4	Zbtb20
	Pcgf3	Strn3	Kcnh7	Zdhhc20
	Plxnd1	Swt1	Kpna4	
	Ppp3ca	Sypl	Kras	
	Pum1	Tab2	Lrp1b	
	Rbms1	Thoc1	March7	
	Rock2	Traf3	Med14	
	Samd12	Trps1	Meis1	
	Snx16	Wnk3	Mier3	
	Stau1	Zbtb20	Myo1d	
	Strn3	Zfp644	Nfe2l2	
	Vangl1		Nfia	
	Zbtb20		Nrp1	
	Zbtb37		Nsun3	
	Zcchc14		POU2F1	
	Zfp827		Prox1	
	Zfr		Ptpn2	

Table S4: Human islet donor information. Related to STAR Methods

				Islets	
	Gender	Age	BMI	Purity (%)	Viability (%)
Donor #1	Male	53	27.2	80	90
Donor #2	Female	39	31.4	70	90
Donor #3	Female	43	34.0	90	95
Donor #4	Male	50	19.6	80	95

Table S5: qPCR Primer Sequences. Related to STAR Methods

	Forward	Reverse
Mouse		
18S	5'-GCA ATT ATT CCC CAT GAA CG-3'	5'-GGC CTC ACT AAA CCA TCC AA-3'
Ccl2	5'-AGG TGT CCC AAA GAA GCT GT-3'	5'-ACA GAA GTG CTT GAG GTG GT-3'
Ccl7	5'-ATC TCT GCC ACG CTT CTG T-3'	5'-TAT AGC CTC CTC GAC CCA CT-3'
Cxcl10	5'-GCC GTC ATT TTC TGC CTC AT-3'	5'-GAT AGG CTC GCA GGG ATG AT-3'
Ear12	5'-TCC CGA CTT TGT CTC CTG TT-3'	5'-TTT CCA CAC ACA CCA ACA GC-3'
Gapdh	5'-TGGCAAAGTGGAGATTGTTGCC-3'	5'-AAGATGGTGATGGGCTTCCCG-3'
Gfp	5'-CTGACCCTGAAGTTCATCTG-3'	5'- GTCGTCCTTGAAGAAGATGG-3'
H2-Eb2	5'-CTC CTG GTC TGC TCT GTG AT-3'	5'-AAC CAT CTC CAG CAT CAC CA-3'
Hprt	5'-AGTCCCAGCGTCGTGATTAG-3'	5'-AATCCAGCAGGTCAGCAAAG-3'
Ifng	5'-GCT ACA CAC TGC ATC TTG GC-3'	5'-TGT CAC CAT CCT TTT GCC AG-3'
Igfbp2	5'-AAG GTC AAT GAA CAG CAC CG-3'	5'-GCT TGT CAC AGT TGG GGA TG-3'
Pf4	5'-AGC TGT GTG TGT GTG AAG AC-3'	5'-TAT ATA GGG GTG CTT GCC GG-3'
Reg3b	5'-TGG TTT GAT GCA GAA CTG GC-3'	5'-CCA TTC CCA TCC ACC TCC AT-3'
Rat		
Ccl2	5'-AGG TGT CCC AAA GAA GCT GT-3'	5'-ACA GAA GTG CTT GAG GTG GT-3'
Ccl7	5'-ATC TCT GCC ACG CTT CTG T-3'	5'-TAT AGC CTC CTC GAC CCA CT-3'
Cxcl10	5'-CCA GTG CTG CTG TCG TTC TC-3'	5'- TCT CAA CAT GCG GAC AGG AT -3'
Hprt	5'-AGTCCCAGCGTCGTGATTAG-3'	5'-AATCCAGCAGGTCAGCAAAG-3'
Human		
CCL2	5' - GCA GCA AGT GTC CCA AAG AA-3'	5'- CTG GGG AAA GCT AGG GGA AA-3'
CCL7	5'- CTT CAA CTA CCT GCT GCT ACA-3'	5'-GGG TTT TCT TGT CCA GGT GC-3'
CXCL10	5' -ACT GTA CGC TGT ACC TGC AT-3'	5'- TGA TGG CCT TCG ATT CTG GA-3'
HPRT	5' - CCC TGG CGT CGT GAT TAG TG-3'	5'- GCT ACA ATG TGA TGG CCT CCC-3'

Table S6: miRNA sponge sequence. Related to Figure 7

	Mature miRNA sequence	Sponge binding sites	
		sense	anti-sense
miR-142-3p	UGUAGUGUUUCCUACUUUAUGGA	TCCATAAAGTACTTACACTACA	TGTAGTGTAAGTACTTTATGGA
miR-142-5p	CAUAAAGUAGAAAGCACUACU	AGTAGTGCTAGAACTTTATG	CATAAAGTTCTAGCACTACT
miR-150	UCUCCCAACCCUUGUACCAGUG	CACTGGTACACCCTTGGGAGA	TCTCCCAAGGGTGTACCAGTG
miR-155	UUAAUGCUAAUUGUGAUAGGGGU	ACCCCTATCACTAAAGCATTAA	TTAATGCTTTAGTGATAGGGGT

Sponge sequence:

sense: 5’ GTCCC TCCATAAAGTACTTACACTACA CCGG ACCCCTATCACTAAAGCATTAA CCGG AGTAGTGCTAGAACTTTATG CCGG CACTGGTACACCCTTGGGAGA CCGG TCCATAAAGTACTTACACTACA CCGG ACCCCTATCACTAAAGCATTAA CCGG AGTAGTGCTAGAACTTTATG CCGG CACTGGTACACCCTTGGGAGA GG 3’

anti-sense: 5’ GACCC TCTCCCAAGGGTGTACCAGTG CCGG CATAAAGTTCTAGCACTACT CCGG TTAATGCTTTAGTGATAGGGGT CCGG TGTAGTGTAAGTACTTTATGGA CCGG TCTCCCAAGGGTGTACCAGTG CCGG CATAAAGTTCTAGCACTACT CCGG TTAATGCTTTAGTGATAGGGGT CCGG TGTAGTGTAAGTACTTTATGGA GG 3’